Chapter 4

Creation of Long-Acting Nanoformulation for Simultaneous Delivery of Drugs with Differential Physicochemical Properties

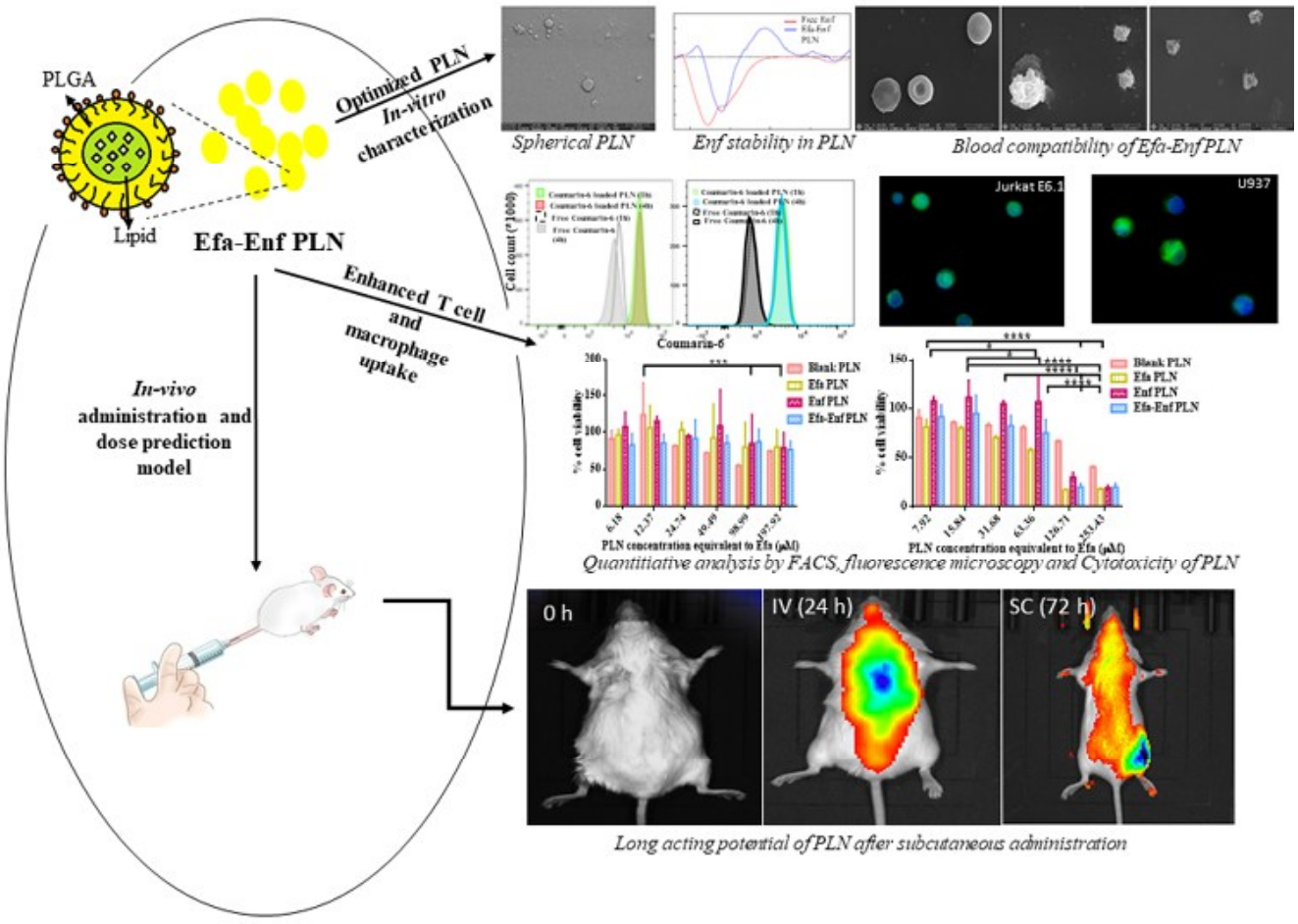

1. Introduction

Oral combination antiretroviral therapy (cART also known as highly active ART or HAART) was invented in 1995 [1] due to consistent attempts for the treatment of life-threatening HIV infection. It consists of two or more drugs from divergent antiretroviral (ARV) class targeting different stages of the HIV life-cycle which enabled increased life expectancy of HIV patients [2]. However, oral cART is associated with drawbacks including frequent dosing [3], inaccessibility, abysmal adherence [4,5], and pruned bioavailability of cART [6] thereby ensuing inadequate therapeutic concentration of cART at inaccessible sites, viral rebound, and drug resistance [7]. Parenteral administration of antiretroviral nanoformulations via subcutaneous (SC) or intramuscular (IM) route may lead to long-term slow effective release for weeks or months by improving pharmacokinetics, biodistribution, and therapeutic efficacy against HIV infection [8,9]. Moreover, long-acting antiretroviral (LA ARV) nanoformulations form primary depot (injection site), secondary depot (infiltered immune cells at administration site or tissue lymphocytes) [10,11] and deliver ARV drugs to the major difficult to access sites (brain and thymus), HIV infection (rectum or vagina), spread sites (lymphatic vessel and lymph node) and reservoir sites (liver and spleen) through lymphatic-circulatory loop [9]. After the successful ATLAS and FLAIR phase III clinical trial, Cabenuva™ containing two long-acting nanocrystal suspensions namely; cabotegravir and rilpivirine have been recently approved by Health Canada for once-monthly administration by intramuscular route [12]. Cabotegravir or rilpivirine loaded LA nanosuspension showed plasma half-life of 25-40 days and 40-days respectively after intramuscular administration to healthy individuals [13]. Profuse preclinical success for LA polymer [14–16] or lipid nanocarriers [17–19] incorporating single or combination ARV have been established for maraviroc, tenofovir, emtricitabine, bictegravir, lopinavir, elvitegravir, atazanavir and ritonavir [9].

Drugs with penurious oral bioavailability, aqueous solubility, rapid first-pass metabolism, and longer half-life are eligible for presentation through LA nanoformulation [9]. To this end, copious hydrophobic drugs with longer half-lives were incorporated into LA nanoformulations which engendered protracted plasma and target tissue drug release [10,20–23]. However, hydrophilic drugs with a short half-life (<10 h), quick elimination, and rapid metabolism have been meagrely explored for the development of LA nanoformulation. Although, delivery of hydrophilic ARV with a median half-life (>10 h) has been developed recently for tenofovir, emtricitabine, and elvitegravir [24–27]; however, combination delivery of drugs with differential physicochemical properties remains at inception. The objective of the present work, therefore, involved the development of LA nanoformulation for co-delivery of drugs with differential physicochemical properties and half-lives. Efavirenz (Efa) is a non-nucleoside reverse transcriptase inhibitor (NNRTI) and is considered under first-line HAART treatment [28]. It exhibits poor aqueous solubility (8.55 µg/ml), log P of 4.6 [29], and rapidly metabolized by first-pass metabolism [30]. Whereas, Enfuvirtide (Enf) is a fusion inhibitor peptide approved by USFDA in 2003 [31]. It is a 36-amino acid peptide with a molecular weight of 4.5 KDa which blocks the fusion of viral and cell membranes by binding to glycoprotein-41 with poor oral bioavailability [32] and rapid catabolism by peptidase and proteinase prominently in hepatic and kidney cells [33,34]. It elicits increased solubility in aqueous buffers (pH 7.5) of 85-142 g/ 100 ml [35], log P of -17.2 [36], and half-life of 3.8 h [37]. Moreover, co-delivery of NNRTI and HIV-1 fusion inhibitor could massively improve anti-HIV effect of individual drugs [38]. Polymeric nanoparticles have precedence due to their hydrophobic nature, long-term stability, narrow polydispersity and surface functionalization potential; yet, encompass drawback including non-biocompatible/ biodegradable, toxicity, poor solubility and penetrability through various biological membrane. Whereas, lipid nanoparticles encompass advantages including higher drug loading, biocompatible, biodegradable, safety,

and low toxicity but, suffer from drawbacks including low stability, drug leakage and difficulty in scale-up [39,40]. Although, diverse polymeric and lipid based nanoparticles were developed to elicit LA potential [9]; however, development of long-acting polymer-lipid hybrid nanoparticles encompassing advantages of both polymeric and lipid system and eliminating their individual drawbacks would lead to enhanced pre-clinical success.

Therefore, the objective of the present study emphasizes on development and optimization Efavirenz (Efa)-Enfuvirtide (Enf) co-loaded polymer-lipid hybrid nanoparticles (PLN) with effective intracellular delivery to immune cells (macrophages and T cells) predominantly responsible for secondary depot genesis. Additionally, it intends to elucidate the biodistribution of LA Efa- Enf co-loaded PLN in Balb/c mice.

2. Materials and methods

2.1 Materials

Efa was a kind gift sample from Ranbaxy Laboratories Ltd. (Gurgaon, India), Enf was purchased from Prospec Protein Specialists (Rehovot, Israel), stearic acid, docusate sodium, dichloromethane, sodium dihydrogen orthophosphate, mannitol was purchased from S D Fine-Chem Limited (Mumbai, India), soy lecithin, dialysis bag (MWCO 12-14 kDa), Dulbecco's phosphate buffer saline and glutaraldehyde (25% w/w) was purchased from HiMedia Laboratories Pvt. Ltd. (Mumbai, India), tween 80, trehalose and thiazolyl blue tetrazolium bromide (MTT) were obtained from Sisco Research Laboratories Pvt. Ltd. (Mumbai, India), cremophor HS-15 was kind gift samples from BASF Chemicals Company (Navi-Mumbai, India). Branched polyethyleneimine (molecular weight-25000), poly(lactic-co-glycolic) acid (PLGA) (50:50), coumarin-6 and cell proliferation WST-1 kit was procured from Sigma-Aldrich Chemicals Company (Missouri, United States). Ficoll-Opaque Plus was procured from GE Healthcare (Chicago, United States). Ethanol from Jabsen and Jabsen Co. (GmbH,

Germany), RPMI 1640, and foetal bovine serum (FBS) were procured from Gibco Biosciences (New York, United States), Phorbol-12-myristate-13-acetate (PMA) was procured from Cayman chemical company. U937, Jurkat E6.1 suspended cell lines and Balb/c mice were kind gifts from ICMR-National Institute for Research in Reproductive Health (Mumbai, India), lactose and sucrose were procured from Central Drug House (New Delhi, India), xenoLight DIR (DilC18(7) or 1,1'-dioctadecyltetramethyl indotricarbocyanine Iodide was procured from PerkinElmer (Waltham, United States) and ultrapurified water was obtained from Milli-Q system (Millipore GmbH, Germany).

2.2 Preparation of Efa-Enf co-loaded PLN

Efa-Enf co-loaded PLN were prepared by a double emulsion solvent evaporation method as described previously with some modifications [41]. Briefly, Efa (50-100 mg) and stearic acid (45 mg) equivalent to 1:1 molar ratio, soy lecithin (200 mg), and PLGA (10 mg) were dissolved in dichloromethane (5 ml) to obtain organic phase. Enf (2 mg) was dissolved in 1 ml of phosphate buffer (10 mM, pH 6.5) and added dropwise to above organic phase and probe sonicated using a probe sonicator (Sonics & Materials, Inc., USA) at 4ºC for 90s (500 watts, 25% amplitude) to obtain w/o primary emulsion. The primary emulsion was then added dropwise to 30 ml of external aqueous phase containing 2% w/v cremophor HS-15 using a homogenizer (IKA® T10 basic Ultra Turrax®) for 600 s at 15000 rpm to obtain w/o/w double emulsion. The organic phase of w/o/w double emulsion was evaporated using Buchi rotoevaporator® at 30ºC for 20 min to obtain aqueous nanodispersion. The aqueous nanodispersion was then probe sonicated for 360 s at 4ºC (500 watt, 25% amplitude) and was stored at 4ºC until further evaluation.

Coumarin-6 and DIR-loaded PLN were prepared by a similar procedure as mentioned above by dissolving coumarin-6 (1 mg) or DIR (0.5 mg) in the organic phase after omitting Efa and Enf

to yield dye loaded PLN. Coumarin-6 and DIR loaded PLN served as surrogate of Efa-Enf PLN to depict cellular uptake and *in vivo* biodistribution studies respectively.

2.3 Optimization of Efa-Enf co-loaded PLN using Box Behnken design

Optimization and statistical analysis of Efa-Enf co-loaded PLN was done by Box-Behnken design using Design-Expert®software version 8.0.7.1 (Stat-Ease Inc., Minneapolis, MN). Based upon initial screening, the three most significant factors namely Efa amount (A), sonication time for o/w primary emulsion (B), and sonication time for w/o/w aqueous nano-dispersion (C) in formation of Efa-Enf co-loaded PLN, were identified. While, amount of Enf (2 mg), stearic acid (45 mg), PLGA (10 mg), soy lecithin (200 mg), cremophor HS-15 (600 mg), dichloromethane (5 ml), external aqueous phase (30 ml) and homogenization speed and time (15000 rpm, 10 min) were kept constant. A valid design space was generated using 3-center points for replication and 12-mid points of each edge of a cube. Three independent factors were varied at three levels as shown in Table 4.1 to generate 15 experimental runs (Table 4.2). The main effect, interaction effect, and quadratic effect of independent factors were observed on dependent factors like Y_1-Efa %EE. Y_2- Enf %EE, Y_3-particle size, and Y_4-polydispersity index (PDI) for Efa-Enf co-loaded PLN and suitable response surface graphs, polynomial equations, and mathematical models were generated. After generating the model based on the relation of independent and dependent factors, each dependent factor or response was optimized based on the desirability function. Validation of the model was performed by matching the predicted and obtained values of dependent factors for specific independent factors of PLN eliciting the highest desirability function.

Table 4.1 Independent and dependent factors in Box Behnken optimization design for Efavirenz-Enfuvirtide co-loaded PLN

	Box-Behnken design			
Independent factors		**Levels**		
		-1	**0**	**+1**
A=Efavirenz amount	mg	50	75	100
B= sonic time for w/o primary emulsion	s	0.30	1.30	3.00
C=sonic time for w/o/w emulsion	min	1.30	3.00	6.00
Dependent factors				
Y_1=Efavirenz % entrapment efficiency	Y_2= Enfuvirtide % entrapment efficiency	Y_3=Particle size		Y_4=PDI

2.4 Characterization of Efa-Enf co-loaded PLN

2.4.1. Particle size, polydispersity index (PDI) and zeta potential

The aqueous nanodispersion of Efa-Enf co-loaded PLN, coumarin-6 loaded PLN and DIR loaded PLN obtained in section 2.2 were centrifuged at 17000 rpm at 4^{o}C for 25 min using Eppendorf, 5430 R centrifuge followed by separation of supernatant from pellets. The pellet was re-dispersed and diluted using Milli Q water. Particle size, PDI, and zeta potential of diluted samples were measured by photon correlation spectroscopy using Malvern Nano ZS (Malverns instrument Ltd., UK) at 30^{o}C.

2.4.2. % Entrapment efficiency (EE)

The supernatant obtained after centrifugation as described above was suitably diluted and analyzed using high-performance liquid chromatography (HPLC) as reported previously by our group [42] and spectrofluorophotometer to determine the amount of Efa and Enf respectively. The %EE was calculated using equation (4.1).

$$\% \text{ entrapment efficiency} = \frac{\text{Total amount of drug added} - \text{amount of drug in supernatant}}{\text{Total amount of drug added}} \times 100 \ldots (4.1)$$

2.4.3. Field-emission Scanning Electron Microscopy (FESEM)

2 mg of lyophilized Efa-Enf co-loaded PLN were placed onto the carbon tape attached to metal stub and gold-coated for 45s using Quorum Technologies Q150TES sputter coater (East Sussex, England). Gold-coated nanoparticles were then analyzed by FEI™ scanning electron microscope (Hilsboro, Washington) at 20KV high vacuum, 60000X magnification with a spot size of 8.0, and scale of 1-3 μm.

2.4.4 Differential scanning calorimetry (DSC)

DSC was performed by DSC-60 Plus by Shimadzu (Kyoto, Japan). DSC thermogram of Efa, Enf, stearic acid, PLGA, soy lecithin, cremophor HS-15, trehalose, and lyophilized Efa-Enf co-loaded PLN was obtained by adding 5 mg of each sample in an aluminium pan and heating individual sample pan at the rate of 10ºC/min between 30-300ºC with an empty aluminium pan as reference under nitrogen purge (20 ml/min).

2.4.5. Fourier transform infrared spectra (FTIR)

FTIR spectra of 10 mg of each Efa, Enf, stearic acid, PLGA, soy lecithin, cremophor HS-15, trehalose, and their physical mixture and lyophilized Efa-Enf co-loaded PLN was recorded by Bruker alpha-one FTIR spectrophotometer (Bruker Optik, Germany) after placing individual sample (5 mg) on ZnSe sample crystal and scanning the spectra from 3800- 600 cm^{-1}.

2.5 Circular Dichroism analysis (CD)

The secondary structure of free Enf and Enf loaded in PLN was analyzed using Jasco circular dichroism instrument (Easton, United States). CD analysis of both the samples was done in

phosphate buffer (10 mM, pH 6.8) at 25°C with a scanning speed of 50 nm/min and 0.1 cm cell length.

2.6 Lyophilization studies

2.6.1 Freeze-thaw studies

Freeze-thaw studies were carried out as a pre-test to screen various cryoprotectants; namely, lactose, sucrose, mannitol, trehalose for lyophilization of Efa-Enf co-loaded PLN. The aqueous nanodispersion of Efa-Enf co-loaded PLN was frozen for 24 h at -80ºC in a deep freezer (Thermo Fischer Scientific, USA) after dissolving individual cryoprotectant (3.2% w/v) in a glass vial. Frozen samples were kept at room temperature for thawing. Particle size and PDI of Efa-Enf co-loaded nano-dispersion were determined as described in section 2.4.1.

2.6.2 Lyophilization studies

The aqueous nano-dispersion of Efa-Enf co-loaded PLN (25 ml) was centrifuged at 48000 rpm for 20 minutes to separate the PLN. Thereafter, PLN were redispersed in 7.5 ml of MilliQ water and frozen at -80ºC in a deep freezer (Thermo Fischer Scientific, USA) for 12 h after dissolving 20% w/v trehalose. Lyophilization was carried out in Labconco freeze drier (FreeZone 2.5, USA) for 48 hours at -54ºC and -0.018 mBar. The lyophilized nanoparticles were reconstituted (30 mg/ ml) with Milli Q water. Particle size, PDI, and zeta potential were determined as mentioned in section 2.4.1. An aliquot of reconstituted nanoparticles was extracted with acetonitrile (800 µl) and bath sonicated for 5 min. Thereafter, the extract was centrifuged at 15000 rpm for 10 min, suitably diluted, and analyzed by HPLC and spectrofluorimetry to determine Efa and Enf content respectively.

2.7 *In vitro* drug release studies

In vitro release of Efa-Enf co-loaded PLN was carried out using the dialysis bag method as described previously [29]. Briefly, Efa-Enf co-loaded PLN dispersion equivalent to 2.1 mg and 34 µg of Efa and Enf respectively, was filled in a dialysis bag (MWCO 12-14 kDa, Himedia Lab. Pvt. Ltd., Mumbai, India). The dialysis bag was closed from both sides and suspended in 30 ml of phosphate buffer (10 mM, pH 7.4) in a shaking water bath (100 rpm, 37^{o}C). 3 ml of sample was withdrawn at pre-determined time-points (0.5, 2, 4, 8, 12, 24, and 33 h) and replaced with an equivalent amount of fresh dissolution medium. The samples were then diluted appropriately and analyzed by HPLC and spectrofluorophotometer to determine the release of Efa and Enf; respectively, from the PLN. The study was carried out in triplicate.

2.8 Blood compatibility studies

2.8.1 *In vitro* hemolysis studies

In vitro hemolysis studies were carried out as reported previously with some modifications [43]. Blood was collected from Wistar rats in tubes containing EDTA solution (10% w/v, blood: anticoagulant ratio of 50:1) and centrifuged at 1000 rpm for 5 min. After centrifugation, the red blood cells (RBCs) were collected and rinsed with normal saline and further centrifuged to obtain RBC pellet. The RBC pellet was then diluted with 200 µl of normal saline. Efa-Enf PLN were suitably diluted with normal saline to obtain a final concentration of Efa and Enf between 20-60 µg/ml and 0.1-0.3 µg/ml respectively. Similar dilutions were made for blank PLN to serve as control. To 100 µl of each dilution, 100 µl above RBC suspension was added and incubated at 37°C for 30 min. Normal saline and distilled water were used as negative and positive control respectively. After 30 min, normal saline was added up to 1 ml. Each sample was centrifuged at 1000 rpm for 5 min and 200 µl of supernatant was analyzed using Epoch

Elisa plate reader (BioTek U.S., Winooskii) at 540 nm. % hemolysis was calculated using equation (4.2).

$$Haemolysis\ (\%) = \frac{\text{ODsample} - \text{ODnegative control}}{\text{OD positive control} - \text{ODnegative control}} * 100 \ldots\ldots\ldots\ldots\ldots\ldots\ldots (4.2)$$

2.8.2 RBC, WBC and platelet aggregation studies

Treated RBC pellet were suitably diluted (20 times in normal saline) and 100 µl RBC suspension was fixed in 100 µl of glutaraldehyde solution (2.5% in normal saline). 50 µl of RBC-glutaraldehyde solution was added onto a glass coverslip and allowed to dry overnight at 4℃. The samples were washed thrice with normal saline, dehydrated with 50%, and 100% ethanol sequentially, and coverslip were allowed to dry at 37℃. The samples were placed onto the carbon tape attached to metal stub and gold-coated for 45s using Quorum Technologies Q150TES sputter coater (East Sussex, England). Gold-coated treated RBC were then analyzed by FEI™ scanning electron microscope (Hilsboro, Washington).

Further, platelet and white blood cells (WBCs) aggregation studies were carried out to evaluate the blood compatibility of PLN. The Platelets and WBCs were separated by layering rat blood suitably diluted with normal saline (1:1 ratio) on 3 ml Ficoll-Paque Plus and centrifuging at 400 g for 30 min. For aggregation studies, 50 µl of WBCs or platelet suspension were treated with 50 µl of Efa-Enf co-loaded PLN equivalent to 40 µg Efa and 0.78 µg Enf at 37°C for 1 h. PEI and normal saline were used as positive and negative control respectively. The treated cells were then prepared for SEM analysis similar to RBCs as stated above [43].

2.9 Cytotoxicity and cellular uptake of Efa-Enf co-loaded PLN

2.9.1 Cells

Jurkat E6.1 T and U937 suspended cell lines were cultured in RPMI 1640 media enriched with FBS (10% w/v) in a T-75 culture flask at 37°C and 5% v/v CO_2 for 6 days until the optimal cell density of $11*10^6$ cells/ml were obtained.

2.9.2 Cytotoxicity studies

2.9.2.1 Cytotoxicity studies in Jurkat E6.1 T cells

Jurkat E6.1 T cells (10^4 cells/well) were suitably seeded in a 96-well plate. The cells were incubated with 50 µl of blank PLN, Efa PLN, Enf PLN and Efa-Enf PLN equivalent to Efa (7.92, 15.84, 31.68,63.36,126.71 and 253.43 µM) and Enf (0.898, 0.449, 0.225, 0.112, 0.056, 0.028 µM) for 24 h. Thereafter, 10 µL of cell proliferation WST-1 reagent was added in each well and incubated for 4h. The 96-well plate was kept on a plate shaker for 10 min. Thereafter, absorbance was recorded at 440 nm using Epoch Elisa plate reader (BioTek U.S., Winooskii).

2.9.2.2 Cytotoxicity studies in U937 cells

U937 macrophage cells (10^5 cells/well) suspended in complete RPMI 1640 media containing PMA (0.1 ng/ml) were seeded in 96 well plate and incubated in a CO_2 incubator (5% v/v CO_2, 37°C) overnight. The media was removed and treated with 100 µl of blank PLN, Efa PLN, Enf PLN and Efa-Enf PLN dispersed in RPMI 1640 media equivalent to Efa (6.18, 12.37, 24.74, 49.49, 98.99 and 197.92 µM) and Enf (0.045, 0.089, 0.179, 0.357, 0.714, 1.42, 2.86, 5.72 µM) for 24h. Thereafter, the supernatant was removed and cells were treated with 100 µl MTT reagent (500 µg/ml) for 4 h, the reagent was removed and 100 µl DMSO was added to dissolve formed formazan crystals. Thereafter, the absorbance was recorded at 570 nm using the Epoch Elisa plate reader (BioTek U.S., Winooskii).

2.9.3 Fluorescence microscopy

Jurkat E6.1 T-cells and U937 macrophage cells (10^6 cell count) were seeded in 1.5 ml microcentrifuge tubes. Thereafter, cells were incubated with 100 µl coumarin-6 PLN suitably diluted with RPMI 1640 medium without FBS to obtain 100 ng/ml coumarin-6 concentration at 37°C for 1 or 4 h in 5% (v/v) CO_2. Thereafter, microcentrifuge tubes were centrifuged at 3000 rpm for 5 min to obtain cell pellet. The pellet was then washed with Dulbecco's phosphate buffer saline (DPBS) twice and counterstained with DAPI (300 ng/ml) by incubating for 15 min in dark. The cells were again washed and resuspended using DPBS, aliquots of which was mounted onto a glass slide and fixed using 4% paraformaldehyde. The cells were then observed under Carl ZEISS Axio fluorescent microscope (Jena, Germany) and images were processed using AxioVisionRel.4.5 software.

2.9.4 Flow cytometry

Coumarin-6 PLN cellular uptake quantification was performed using a flow cytometer. Cells (10^7) were incubated with 100 µL of free coumarin-6 or coumarin-6 PLN in DPBS at 37°C for 1 and 4 h and analyzed by FACS Aria SORP with Argon laser (Becton Dickinson, San Jose, CA, USA). A total of 10000 events were recorded in the flow cytometer and cell sorter (FACS). The data was analyzed using DIVA 6.1.3 software (BS, San Jose, CA, USA).

2.10 *In-vivo* biodistribution

All animal procedures were approved by the Institutional Animal Ethics Committee of National Centre for Preclinical Reproductive and Genetic Toxicology ICMR, National Institute for Research in Reproductive Health, Parel, Mumbai (Protocol no.: IAEC no 14-19). Female Balb/c mice 8-12 weeks old were utilized for the study. The animals were divided into 4 groups. DIR PLN were administered to the group I intravenously via tail vein and

subcutaneously via the right flank to group II, III, and IV. Whole-body imaging was carried by Perkin Elmer IVIS Lumina S5 (Waltham, United States) at pre-determined time point for group I (0, 1, 2, 4, 8, 10 and 24 h), group II (0, 1, 2, 4, 8, 10, 24 and 48 h), group III (0, 1, 2, 4, 8, 10 and 72 h) and group IV (0, 1, 2, 4, 8, 10, 24, 48, 72, 96 and 120 h). Animals were sacrificed after 24h of group I and II, 72 h of group III, and 120 h of group IV. The fluorescence intensity of different organs including brain, heart, kidneys, liver, lung, axillary lymph nodes, spleen, thymus, female reproductive tract (FRT) was measured using PerkinElmer IVIS Lumina S5 (Waltham, United States).

2.11 Prediction of dose and target site drug level by simulation of DIR PLN biodistribution profile

The *in- vivo* biodistribution of DIR PLN was used as surrogate wherein, a fraction of DIR PLN reaching various tissues was utilized to predict the dose of Efa and Enf PLN required to achieve MEC of individual drug using equation (4.3).

$$predicted\ dose\ (\mu g) = \frac{MEC\ (\mu g/ml)}{available\ fraction\ mean\ of\ DIR\ PLN/gram\ organ\ weight} X blood\ volume\ per\ gram\ target\ tissue\ weight\ \left(\frac{ml}{g}\right) \ldots \quad (4.3)$$

2.12 Statistical analysis

Statistical data analysis was performed using a student t-test with $p<0.05$ as a minimal level of significance. The results were expressed as mean±standard deviation (SD) obtained from three separate experiments (n=3). Mathematical fit functions were performed by ANOVA analysis.

3. Results and Discussion

3.1 Optimization of Efa-Enf co-loaded PLN using Box Behnken design

Box-Behnken design is a 3^{k-p} fractional factorial design that comprises of the higher number of runs with a high degree of freedom and precise optimization. Further, the design is spherical and rotatable which aid in orthogonal blocking. Therefore, the main effect, interaction effect, and quadratic effect of each independent variable viz, Efavirenz amount (A), sonication time for w/o primary emulsion (B), and sonication time for aqueous nano-dispersion (C) were examined on %EE of Efa (Y_1), %EE of Enf (Y_2), particle size (Y_3) and PDI (Y_4) (Table 4.2).

Table 4.2 Responses obtained from experimental runs of Efavirenz-Enfuvirtide co-loaded PLN by Box-Behnken optimization design

Run	A (mg)	B (min)	C (min)	Efavirenz % EE	Enfuvirtide % EE	Particle size (nm)	PDI
1	50	1.30	1.30	5.2±3.29	29.1±11.58	372.8±17.11	0.454±0.09
2	75	1.30	3.00	28.9±6.47	70.4±9.10	346.3±16.61	0.472±0.03
3	75	3.00	6.00	22.9±10.71	61.2±7.57	395.7±15.20	0.266±0.01
4	75	3.00	1.30	21.7±3.99	54.0±3.60	494.3±89.02	0.502±0.03
5	50	3.00	3.00	24.6±7.56	8.7±4.49	308.1±21.66	0.283±0.03
6	50	0.30	3.00	11.6±6.96	35.2±15.00	369.2±5.95	0.522±0.04
7	75	0.30	1.30	20.4±10.04	64.3±3.95	512.9±34.76	0.532±0.05
8	100	0.30	3.00	18.3±2.81	66.8±6.91	483.2±97.27	0.569±0.03
9	50	1.30	1.30	14.3±3.01	39.1±8.45	410.2±56.38	0.510±0.06
10	100	1.30	6.00	23.2±8.29	78.6±3.74	363.6±25.73	0.405±0.06
11	100	3.00	3.00	26.9±6.95	60.9±5.89	356.2±12.58	0.431±0.08
12	75	1.30	3.00	22.0±3.88	70.2±7.10	369.8±15.53	0.430±0.03
13	100	1.30	1.30	27.0±7.91	75.2±4.55	597.3±38.39	0.572±0.03
14	75	0.30	6.00	3.1±4.56	63.0±7.95	360.4±5.42	0.432±0.03
15	75	1:30	3.00	23.5±1.01	64.1±8.07	377.3±20.64	0.477±0.03

(Data represents mean± S.D, n=3)

The quadratic model was significant for Y_2 (R^2–0.9817) and Y_3 (R^2–0.932) while, a linear model with an insignificant lack of fit was established for Y_1 (R^2-0.6225) and Y_4 (R^2-0.7596) to navigate the design space. Further, every factor was found to have a significant impact ($p<0.05$) on each dependent factor as determined by ANOVA (Table 4.3).

The first-order polynomial equations obtained for the response Y_1 and Y_4 were as follow:

$Y_1=20.274+4.9878A+4.069*B-2.379*C$……(4.4)

$Y_4= 0.4571+0.026*A-0.072*B-0.07*C$……..(4.5)

The negative effect (negative coefficient in the linear equation) on Y_1 and Y_4 was observed with increasing sonication time of double emulsion due to an increase in the total energy of the system leading to increased drug expulsion and decrease in PDI of the PLN which is in agreement with previous reports [44,45]. While the second-order polynomial equation (4.6) and (4.7) for Y_2 and Y_3 signify that the single coefficient terms depict the main effect and the combination term indicates the interaction effect. The coefficient of C is lowest and hence exerted an insignificant effect on response Y_2. While the coefficient of combination term A*B and A*C is highest and thus have a profound effect on Y_2 and Y_3 respectively.

$Y_2=64.18+21.16*A-5.561*B-0.097*C+5.1483*A*B+3.3375*A*C+2.1443*B*C-15.21A^2-10.1B^2+2.5068*C^2$……(4.6)

$Y_3=360.375+42.518*A-21.42*B-65.27*C-16.47*A*B+49.06*A*C+13.5*B*C+4.9399*A^2+9.7984*B^2+66.602*C^2$……(4.7)

Table 4.3. Analysis of Box-Behnken experimental design for Efavirenz-Enfuvirtide co-loaded PLN by ANOVA

Response	Source	Sum of squares	df	Mean square	F value	p-value (Prob>F)
Efavirenz % EE	Model	376.7429	3	125.581	6.0456	0.0110
	Residual	228.4938	11	20.7722		
	Lack of fit	202.4874	9	22.4986	1.7302	0.4194
	Pure error	26.0064	2	13.0032		
	Cor total	605.2367	14			
Enfuvirtide % EE	Model	5218.647	9	579.8496	29.7455	0.0008
	Residual	97.4683	5	19.4937		
	Lack of fit	72.4052	3	24.1351	1.9256	0.3597
	Pure error	25.0631	2	12.5315		
	Cor total	5316.115	14			
Particle size	Model	80118	9	8902	7.6177	0.0189
	Residual	5842.9	5	1168.6		
	Lack of fit	5319.7	3	1773.2	6.7789	0.1313
	Pure error	523.17	2	261.58		
	Cor total	85960	14			
PDI	Model	0.0855	3	0.0285	11.583	0.0010
	Residual	0.0271	11	0.0025		
	Lack of fit	0.0257	9	0.0029	4.2914	0.203
	Pure error	0.0013	2	0.0007		
	Cor total	0.1126	14			

It was observed that at a fixed level of sonication time for aqueous nano-dispersion, Y_1 and Y_4 increased with an increase in both Efa amount and sonication time for w/o primary emulsion. Increased sonication of primary emulsion caused optimum emulsification of amorphonized Efa with lipid in primary emulsion causing efficient particle interaction and enhanced solubilization of Efa in soy-lecithin making drug leakage evitable [46,47]. On the contrary, the aftermath of increased energy of the w/o primary emulsion was enhanced instability (increased Y_4) [48]. An increase in sonication time of w/o primary emulsion at a fixed level of sonication time for aqueous nano-dispersion led to a decrease in the encapsulation of Enf while an increase in Efa amount led to an increase in encapsulation of Enf due to reduced diffusion of drug through the hydrophobic core.

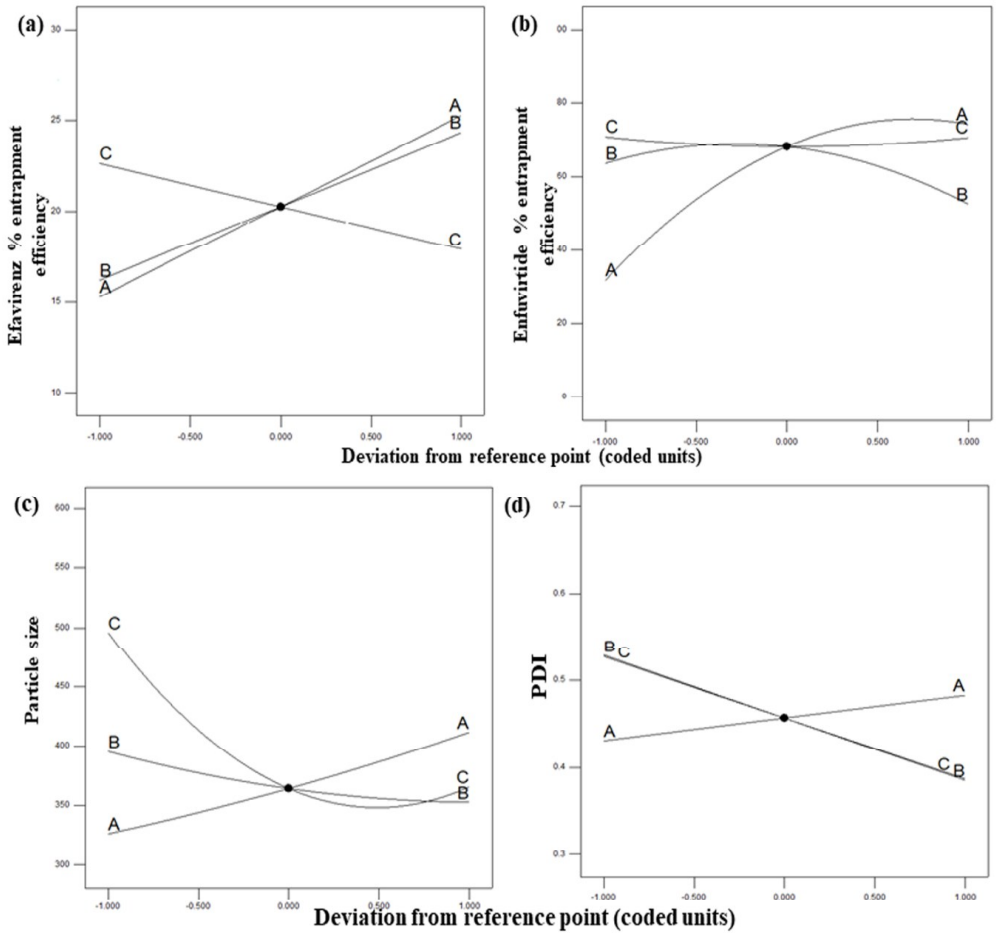

Figure 4.1 Perturbation plot for (a) % EE of Efavirenz (b) % EE of Enfuvirtide (c) particle size (d) PDI (A-Efavirenz amount, B-sonication time for primary emulsion, C-sonication times for aqueous nanodispersion).

The main effect of an independent factor on individual response was analyzed by perturbation plots (Figure 4.1) while, 3D model graphs were used to determine the interaction effect of two independent variables on dependent factors at a fixed level of the third independent variable (Figure 4.2).

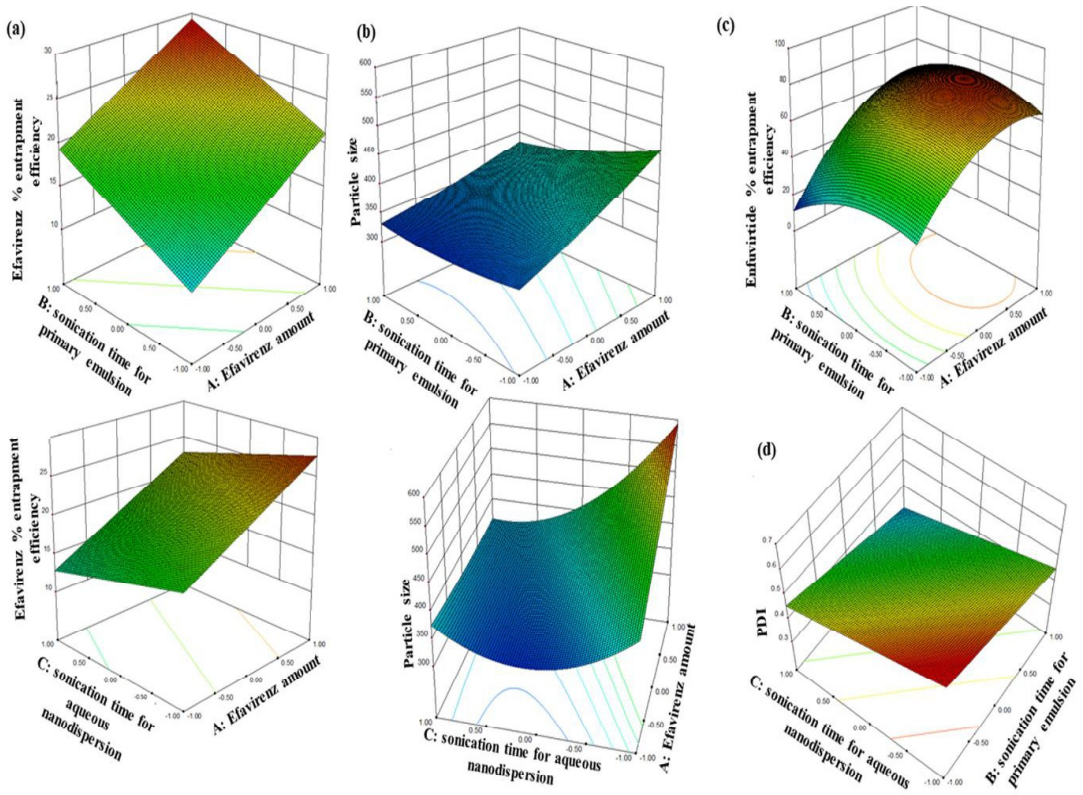

Figure 4.2 Box Behnken 3D response surface plot (a) % EE Efavirenz (b) particle size (c) % EE Enfuvirtide (d) PDI.

On the other hand, the sonication time of aqueous nano-dispersion depicted inverse relation with Y_2, Y_3, and Y_4. However, higher collisional frequency of PLN accompanied by an increase in total energy w/o/w aqueous nanodispersion; increased particle size, and PDI after a specific level [48]. Whereas, Particle size of PLN increased with an increase in Efa due to enhanced encapsulation of Efa [49].

The optimal solution was obtained by setting the target of Efa amount and sonication time for w/o primary emulsion in range, the target for sonication time for aqueous nano-dispersion was set at 0 level to achieve stable PLN with the goal of minimum error propagation of Enfuvirtide and particle size, minimum standard error, maximum % EE of Efa and Enf and minimum particle size and PDI.

The solution obtained with desirability next to 1 (D=0.883) with optimized level for each factor being 0.83, 1, and 0.20 for Efavirenz amount, sonication time for primary emulsion and sonication time for aqueous nano-dispersion respectively was adopted and screened to calculate % bias between predicted and actual values (Table 4.4). The % drug loading of Efa and Enf in the optimized Efa-Enf PLN was found to be 10.4%±0.29% and 0.53%±0.031%, respectively.

Table 4.4 Validation of Box-Behnken design for Efavirenz-Enfuvirtide co-loaded PLN

Parameter	Predicted	Actual	Mean % bias
Efavirenz % EE	28.0	27.1±0.78*	3.12
Enfuvirtide % EE	64.9	69.7±3.79*	7.2
Particle size (nm)	362.2	346.4±30.41*	4.4
PDI	0.39	0.440±0.06*	11.9

(*Each value represent mean±SD, n=3, $p<0.001$ for one-tailed paired t-test)

The optimized solution was utilized to prepare surrogate PLN as described in section 2.2 for cellular uptake and *in-vivo* biodistribution studies (Table 4.5).

Table 4.5 Particle size, PDI and zeta potential of surrogate PLN

Surrogate PLN type	Particle size (nm)	PDI	Zeta potential (mV)
Coumarin-6 PLN	161.1±13.34	0.359±0.004	-42.8±2.14
DIR PLN	212.5±31.79	0.332±0.06	-46±0.28

Each data represented as mean±SD, n=3

3.2 Characterization of Efa-Enf co-loaded PLN

DSC thermograms of different components of PLN and Efa-Enf co-loaded PLN are presented in Figure 4.3(a)**.** It revealed sharp endothermic peaks of stearic acid, PLGA, Efa, and cremophor HS-15 at 59.3ºC, 41.4ºC, 139.3ºC, and 30.5ºC respectively corresponding to their melting point [50–52]. Enf and soy lecithin exhibited a broad peak at 25.8ºC and 158.1ºC corresponding to Enf denaturation and amorphous nature of soy lecithin respectively. Trehalose exhibited three distinct peaks corresponding to the melting peak of dihydrate and anhydrous trehalose at 102.4ºC and 120.8ºC respectively, while the peak at 214.9ºC could be for β-form of anhydrous trehalose as reported previously [53]. The absence of characteristic peaks of individual components of PLN except trehalose indicated an amorphous state of components in PLN [54,55].

FTIR spectra of lyophilized Efa-Enf co-loaded PLN (Figure 4.3(b)) and physical mixture of Efa-Enf PLN components depicted -OH stretch at 3851 $cm^{-1}$and 3741 cm^{-1} similar to PLGA, cremophor HS-15, stearic acid, Enf and Efa, peak at 2922 cm^{-1} and 2852 cm^{-1} corresponding to -CH and -CH_2 stretching, 2361 cm^{-1} corresponding to -C=O stretch as present in stearic acid, PLGA and cremophor HS-15, 1744 cm^{-1} corresponding to the presence of ester as depicted in PLGA, peak at 1653 cm^{-1} and 1461 cm^{-1} corresponding to the dihydrated form of trehalose [56]. Slight shift was observed in IR fingerprint region peaks compared to corresponding excipients. However, the absence of any extra peak confirmed no interaction between the ingredients utilized for the preparation of PLN [29]. Furthermore, FESEM analysis of prepared Efa-Enf co-loaded PLN revealed the spherical shape of nanoparticles (Figure 4.4(a)).

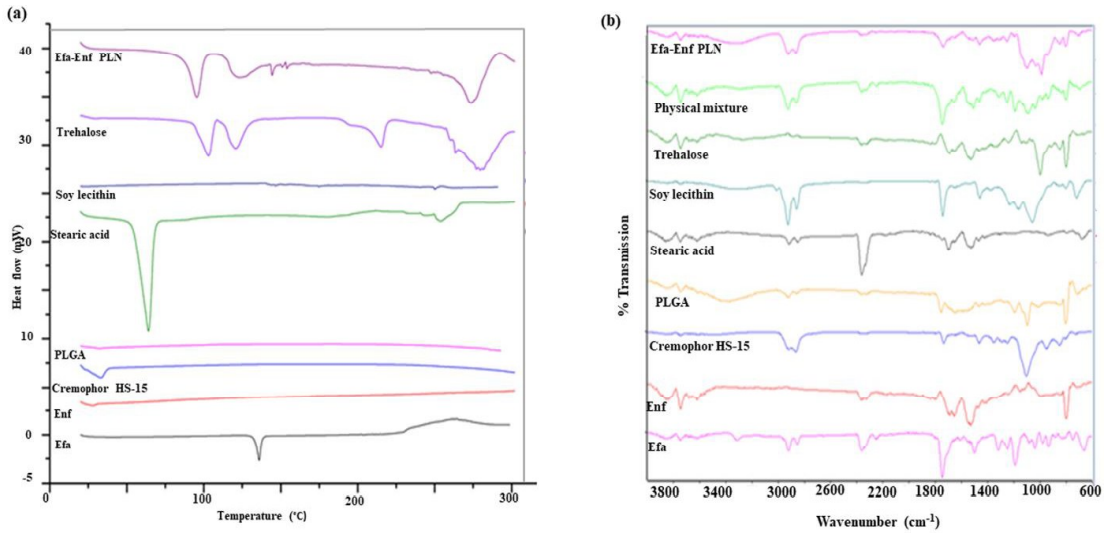

Figure 4.3 *In vitro* characterization of Efavirenz-Enfuvirtide co-loaded PLN (a) DSC thermogram. (b) FTIR.

3.3 CD analysis

CD is most widely used to study the secondary structure of protein and peptide wherein every conformation of protein namely, α-helix, β-sheet, and random coiling leads to unique CD spectra. In the far UV region (190-230 nm) the amide secondary conformation of protein and peptide absorbs circularly polarized light to a different extent. The CD spectra of α-helix leads to two minima at 208 nm (π- π*) and 222 nm (n- π*) while it exhibits a maxima at 191-193 nm (π- π*).CD spectra of Enf and Efa-Enf co-loaded PLN is presented in Figure 4.4(b). It confirmed the presence of α- helix form of Enf after encapsulation into nanoparticles, however, redshift was observed in spectra of Efa-Enf co-loaded PLN which could be due to the interaction of Enf with PLN[57]. The α-helix of Enf is essential for the insertion of Enf into the viral membrane to prevent viral fusion with cell membranes. The results indicated that the encapsulation of Enf in PLN did not affect the secondary structure of the peptide, thereby confirmed maintenance of the antiviral activity of the peptide.

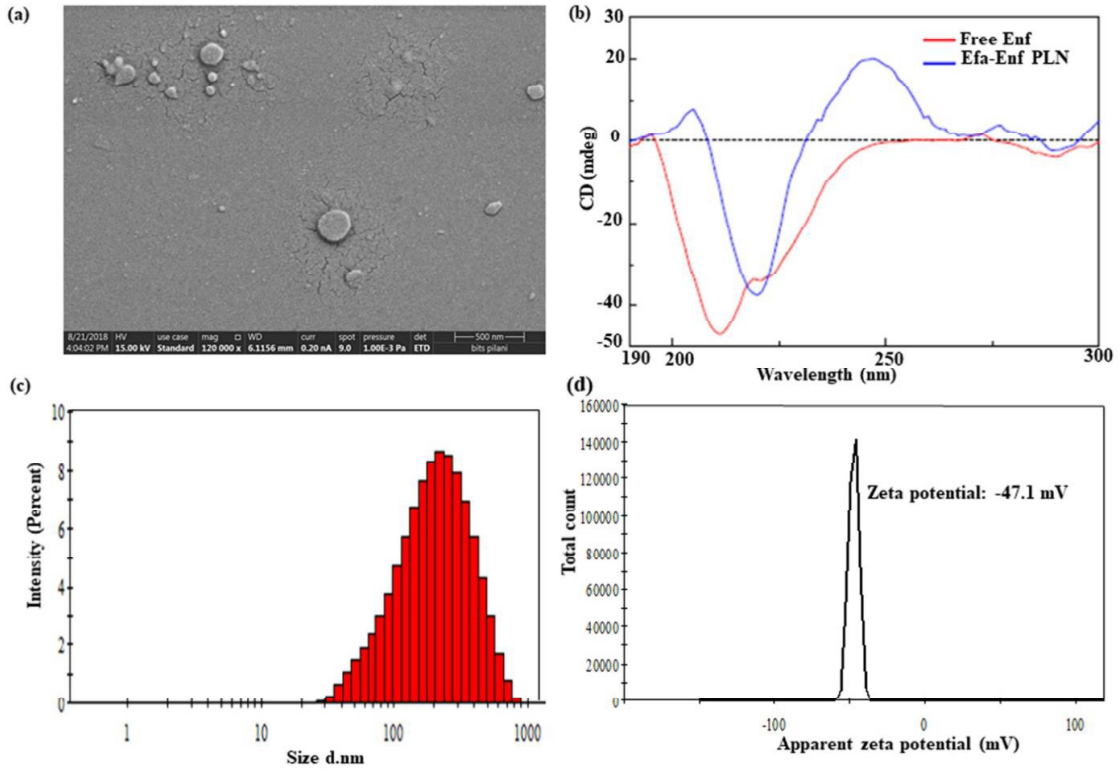

Figure 4.4 *In vitro* characterization of Efavirenz-Enfuvirtide co-loaded PLN (a) SEM image (b) Circular dichroism spectra of free Enfuvirtide and lyophilized Efavirenz-Enfuvirtide co-loaded PLN (c) Particle size and (d) zeta potential of optimized Efavirenz-Enfuvirtide co-loaded PLN

3.4. Lyophilization studies

The impact of lactose, sucrose, mannitol, and trehalose on the physical stability of the PLN during lyophilization was evaluated by freeze-thaw studies. The ratio of final particle size after thawing to initial particle size before freezing of PLN nano-dispersion (S_f/S_i) was calculated (Figure 4.5(a)). It has been reported that S_f/S_i ratio<1.3 indicates good colloidal stability of nanoparticles. The characteristic features of trehalose including selective ability to reduce the dynamics of water, higher glass transition temperature, absence of internal hydrogen bond enhances its ability to bind a higher number of water molecules thus, making segregation of nano-dispersion evitable [58]. Therefore, trehalose was utilized for the lyophilization of Efa-Enf co-loaded PLN. Lyophilized Efa-Enf co-loaded PLN appeared amorphous and bulky

powder (Figure 4.5(b)). It revealed S_f/S_i ratio of 1.1±0.09 with Efa and Enf content of 39.1±5.23 µg/mg and 0.2±0.02 µg/mg respectively.

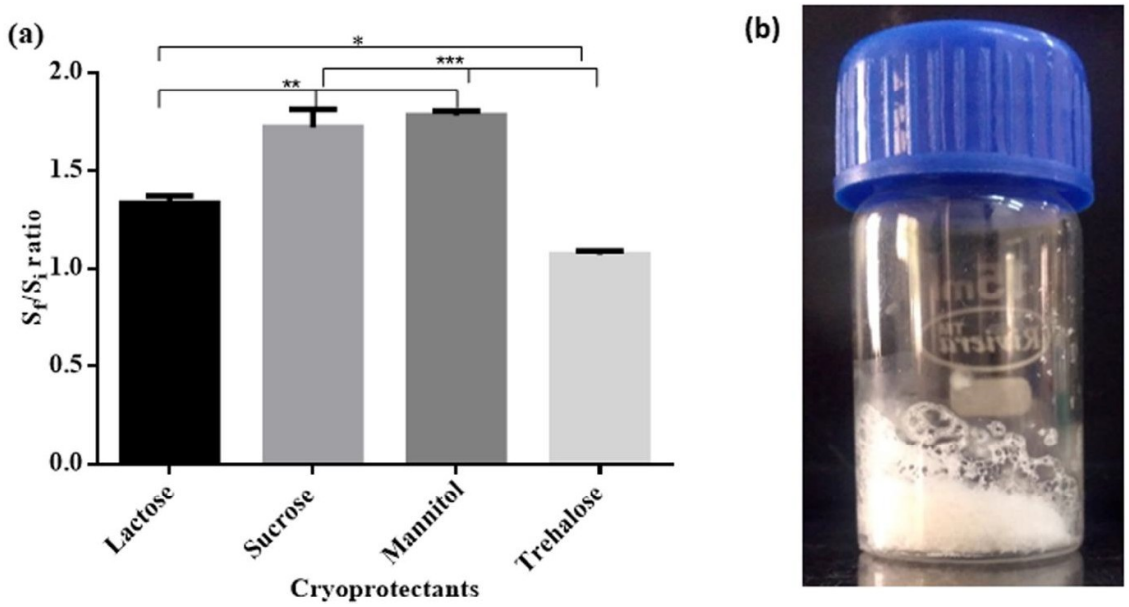

Figure 4.5 Lyophilization studies (a)Freeze thaw studies for screening cryoprotectants for Efavirenz-Enfuvirtide co-loaded PLN (Data represents mean±SD, n=3, * indicates $p<0.05$, ** indicates $p<0.001$ at 95% confidence interval for one-way ANOVA followed by Tukey's multiple comparison test) (b) Pictorial representation of lyophilized Efavirenz-Enfuvirtide co-loaded PLN

3.5 *In vitro* drug release studies

The rate and extent of drug available at the site of action depends upon the rate of drug release from the nanoformulation of cART. Therefore, sustained-release of the drugs from the nanoparticles is desirable to maintain the therapeutic drug level for weeks/months at the target site. Efa-Enf co-loaded PLN revealed sustained-release of Efa and Enf in phosphate buffer solution (pH 7.4) at 37ºC. 15.2±3.36% of free Efa and 79.4±2.26% of free Enf were released at the end of 30 min. While, 8.1±1.30% and 83.4±3.70% of Efa and Enf were released from PLN respectively in 24h, confirming the sustained release potential of PLN (Figure 4.6(a)). Higher drug release of Enf could be due to the opening of pores formed by rapid dissolution or leaching of trehalose and lipid (porogen) upon addition of water thereby, emanating faster

release of hydrophilic drugs [59]. The minimum effective concentration (MEC) required to elicit the anti-HIV effect of Enf (3.8 µg/ ml) [60] is 4-fold higher compared to Efa (<1µg/ml) in cART[61] which is well reflected in the release profile of Efa and Enf from PLN wherein drug release at every time-point of Enf is 5.0-10.2 folds higher compared to Efa. Also, Enf has a higher EC_{50} value (6-91 nM) [62] compared to Efa (EC_{50}-2 nM) and acts by inhibiting the first step of viral infection which involves the restraining fusion of HIV and host cell membrane [63], therefore, higher drug release of Enf compared to Efa would lead to the presentation of the drug combination in a desired fashion to the viral cell.

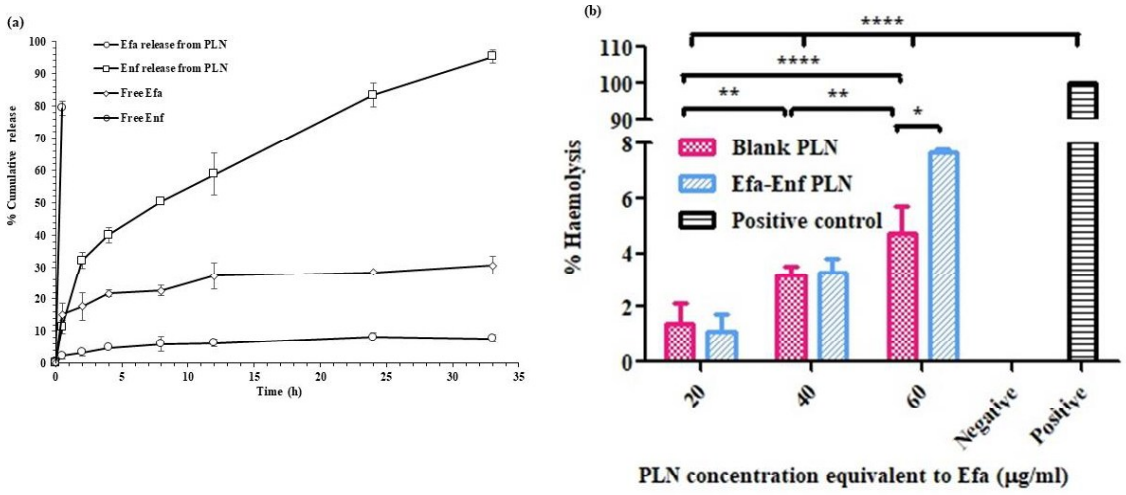

Figure 4.6 *In vitro* drug release and haemolysis studies (a) Release profile of Efavirenz-Enfuvirtide co-loaded PLN (b) Percentage haemolysis of blank and Efavirenz-Enfuvirtide co-loaded PLN (Data represents mean±SD, n=3, * indicates $p<0.05$, ** indicates $p<0.001$, **** indicates $p<0.0001$ at 95% confidence interval by two-way ANOVA)

Thus, differential drug release of Efa and Enf might lead to synergistic killing of HIV [64]. Similar reports have been established for hydrophilic Tenofovir with only 10% of the dose available for lymphatic uptake and 90% in free form was detectable in plasma up to 336 h with initial peak 1h post-administration [11]. Thus, it can be contemplated that Enf released (83%) within 24 h would pass into the blood circulation due to permissible smaller fenestration of blood capillaries from subcutaneous spaces. While the 17% of Enf present into PLN may enter

the lymphatic vessel and trapped into the lymphocytes of the lymph node sinuses thereby creating a depot causing the slow release of Enf and maintaining the therapeutic concentration for a longer duration. However, an *in vivo* proof of concept is yet to be established to confirm the significance of the above differential drug release.

3.6 *In vitro* haemolysis and blood compatibility studies

Depending on size and composition, nanoparticles could exert hemolysis after reaching into the systemic circulation. Therefore, the assessment of the haemolytic potential of formulations is desirable. Blank PLN showed non-haemolytic (<2%) to slightly hemolytic (2-5%) potential as per ASTM acceptable limits. At lower concentrations, the difference in %haemolysis of blank and drug-loaded PLN was not significant. While at higher concentration hemolysis increased to 7.7±0.11% compared to 4.7±1.00% of blank PLN (Figure 4.6(b)). However, %haemolysis of blank and drug-loaded PLN depicted poor hemolytic potential of PLN (<10%) over the entire concentration range [65]. Further, SEM images of RBCs after treatment with blank and Efa-Enf PLN did not cause morphological change in RBCs (Figure 4.7). RBC indices and anaemia are precursors for HIV-1 associated neurocognitive disorder (HAND) [66]. Furthermore, RBC aging and their disposition in the spleen are portent by spicules formed on the cell surface (echinocytes) [67,68]. Thus, the absence of morphological changes in RBCs is a prerequisite in HIV. SEM image of RBCs treated with Efa-Enf co-loaded PLN, blank PLN, and normal saline (negative control) portrayed healthy biconcave shaped RBC morphology, while positive control images revealed irregular morphology with pore formation and echinocytes.

Further, the surface characteristic of nanoparticles may also lead to the initiation of inflammatory response leading to platelet aggregation and thrombosis. Therefore, platelets and WBCs of rat blood were treated with Efa-Enf PLN equivalent to 40 µg and 60 µg Efa and 0.785 and 0.942 µg Enf. Agglutinated and aggregated WBCs and platelets were observed in

PEI treated cells (positive control) (Figure 4.7). However, PLN treated cells were equivalent to normal saline-treated cells, confirming the compatibility of PLN with platelet and WBC.

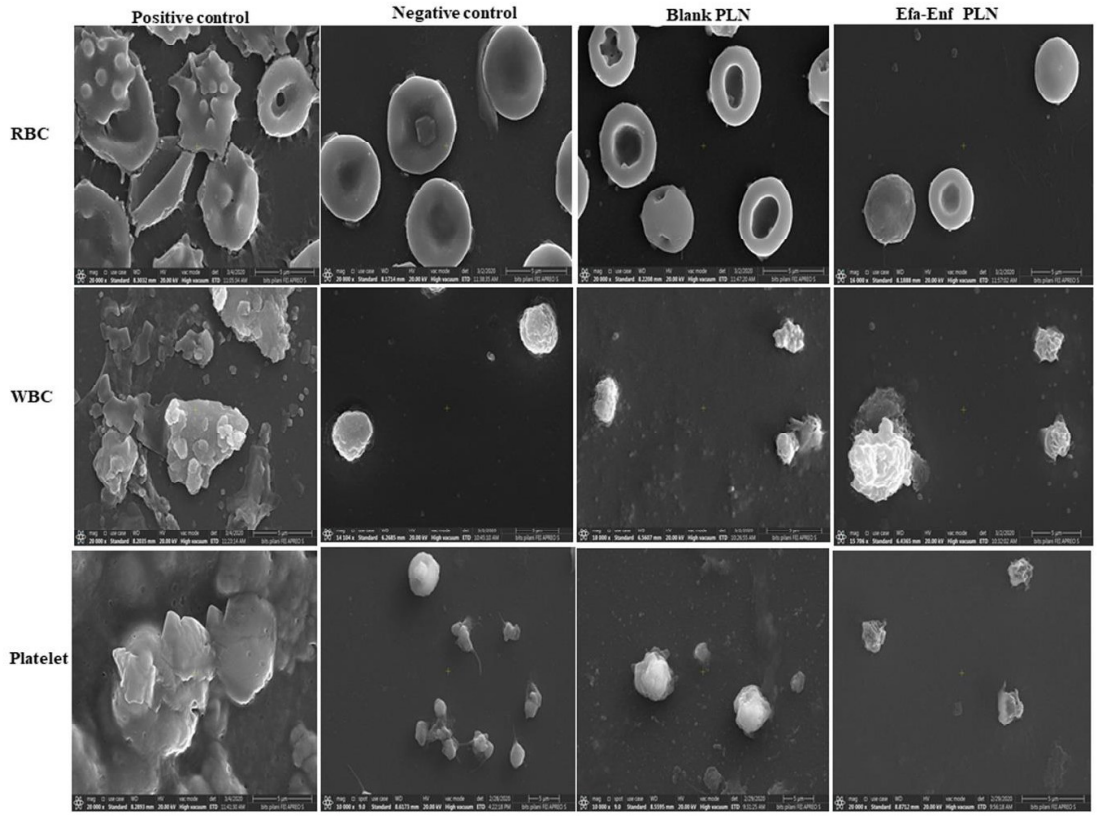

Figure 4.7 Scanning electron micrographs depicting morphology of RBC, platelet and WBC after treatment with blank PLN and Efavirenz-Enfuvirtide co-loaded PLN

3.7 Cytotoxicity and cell uptake studies

Recrudescence of HIV-1 infection occurs due to latently infected viral sanctuaries in immune cells including macrophage and T-lymphocytes [69]. The development of LA ARV nanoformulations led to secondary depot into these sanctuaries [10,11]. Moreover, T cells are prone to the cytopathic effect of HIV-1, unlike macrophages [70]. Thus, cytotoxicity of LA ARV nanoformulations should be studied to avoid catastrophe in immunocompromised individuals. Insignificant difference in % cell viability of Jurkat E6.1 T and U937 cells was observed among blank PLN, Efa PLN, Enf PLN, and Efa-Enf PLN ($p > 0.05$) (Figure 4.8). The

cell viability was >50% for PLN equivalent to 7.92-63.36 µM and 6.18-197.92 µM Efa when tested in Jurkat E6.1 T and U937 cells respectively (Figure 4.8). The reported EC_{50} value for Efa and Enf were found to be 10 nM and 20 nM respectively against HIV-1 infected macrophages as per US federal drug administration [69]. However, the cell viability of Efa-Enf PLN was >75% in U937 macrophage cells at significantly higher concentration than their established EC_{50} value.

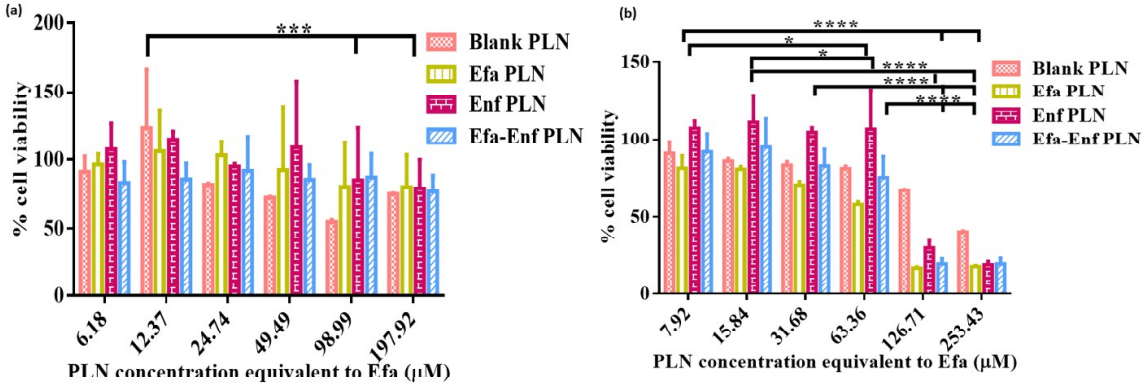

Figure 4.8 Cytotoxicity studies (a) WST-1 cytotoxicity studies in Jurkat E6.1 T cells and (b) MTT cytotoxicity studies in U937 macrophage cells after treatment with blank PLN, Efavirenz PLN, Enfuvirtide PLN and Efavirenz-Enfuvirtide co-loaded PLN (Each data represents mean±SD, n=3, * represents $p<0.05$ and ** represents $p<0.001$, **** represents $p<0.0001$ for two-way ANOVA followed by Tukey's multiple comparison test)

Cellular uptake of PLN was studied by flow cytometry (Figure 4.9) and fluorescence microscopy (Figure 4.10) in Jurkat E6.1 T and U 937 macrophage-like cells by replacing Efa and Enf with coumarin-6. The uptake of coumarin-6 loaded PLN was significantly higher ($p<0.0001$) compared to free coumarin-6 at 1 and 4 h in both Jurkat E6.1 T and U937 cells. Coumarin-6 PLN exhibited 7.5- and 3.8-folds enhanced uptake in Jurkat E6.1 T cells at 1 and 4h respectively as compared to free coumarin-6 (Figure 4.9(a)). While 3.5- and 3.9- folds increased Coumarin-6 PLN uptake was observed compared with free Coumarin-6 at 1 and 4 h respectively in U937 macrophage-like cells (Figure 4.9(b)). However, the cellular internalization at 1 and 4 h was constant ($p>0.05$) for free coumarin-6 and coumarin-6 PLN in

both the cell suspension. Interestingly, the cellular uptake of Coumarin-6 PLN was significantly higher in difficult to target Jurkat E6.1 T cells compared with U937 macrophage cells at both 1h and 4h respectively ($p<0.0001$) as against free Coumarin-6 which showed significantly higher uptake in Jurkat E6.1 T cells only at 4 h ($p=0.0004$).

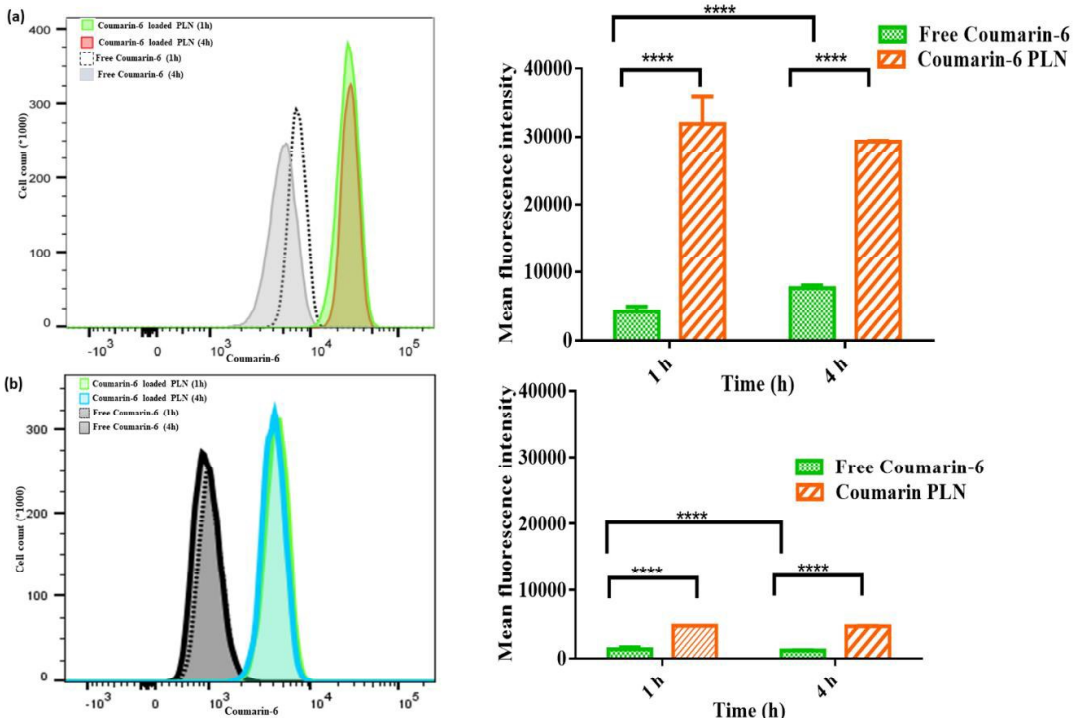

Figure 4.9 Cell uptake studies. (a) Histogram and quantitative time-dependent cellular uptake of free Coumarin-6 and Coumarin-6 PLN in Jurkat E6.1 T cells. (b) Histogram and quantitative time-dependent cellular uptake of free Coumarin-6 and Coumarin-6 PLN in U937 macrophage-like cells. Data expressed as mean±SD, **** : indicates $p<0.0001$ with a 95% confidence interval for two-way ANOVA followed by Tukey's multiple comparison test.

Enhanced T cell uptake of Coumarin-6 PLN could be attributed to particle size independent lipid trafficking pathway. Moreover, T cells consist of cholesterol-dependent glycolipid invaginations responsible for hydrophobic lipid and protein trafficking[71]. Also, many viruses consist of plasma membrane-derived lipid coating and enter the uninfected T-lymphocytes by membrane fusion [72]. Moreover, particle size (>200 nm) along with hydrophobic surface could have contributed to intracellular delivery in macrophage cells. Fluorescent microscopy

study revealed uptake of coumarin-6 PLN in Jurkat E6.1 T-cells and U937 macrophage cells (Figure 4.10).

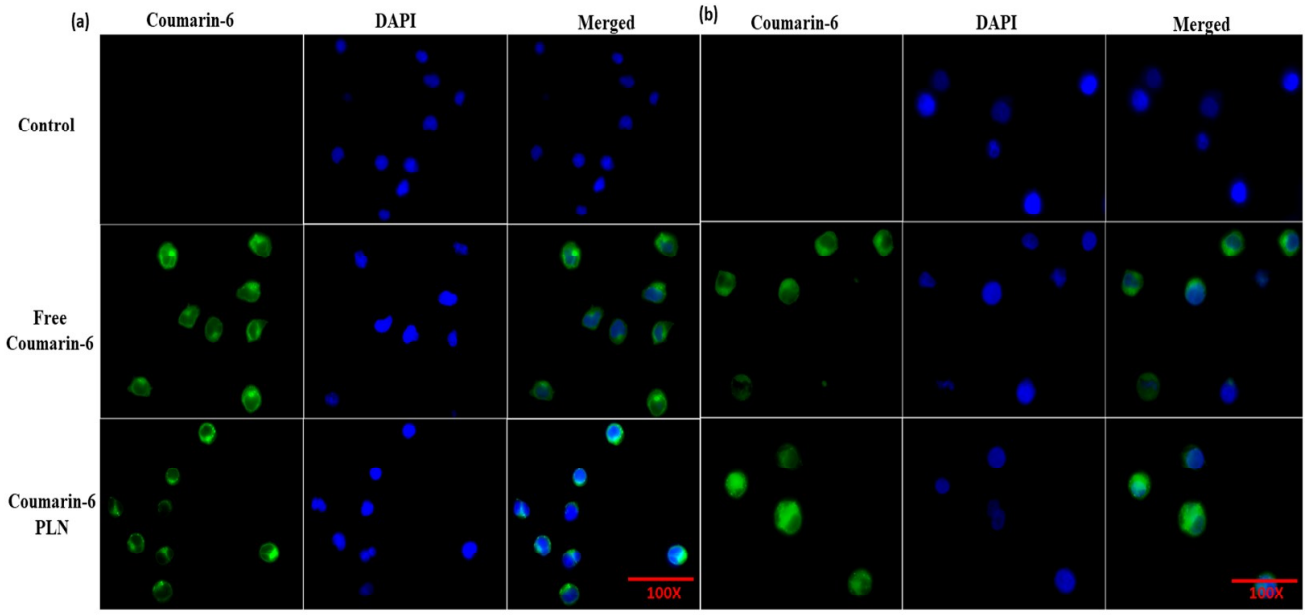

Figure 4.10 Cell uptake studies by fluorescent microscopy after treatment with free Coumarin-6 and Coumarin-6 PLN and counterstaining with DAPI at 1 h in (a) Jurkat E6.1 T cells and (b) U937 macrophage cells.

3.8 *In vivo* biodistribution

Immune cell secondary depot has been established for LA ARV upon parenteral administration. For instance, intravenous (IV) infusion of Ibalizumab monoclonal antibody (2000 mg loading dose followed by 800 mg maintenance dose every 14 days) leads to CD4 T cell receptor occupancy at up to 25 weeks [73]. Therefore, DIR PLN (Efa-Enf co-loaded PLN surrogate) upon IV administration might have led to omnivorous immune cell depot which was carried to various organs preceding distribution to the liver as depicted by higher accumulation in the liver compared with other organs (1, 2, 4, 8, 10 and 24 h) and initiation of non-uniform

biodistribution throughout the body within 2 h post administration and leading to tissue-specific immune cell depot (Figure 4.11(a)). Infected blood monocytes and Kupffer cells

(differentiated macrophage) of the liver consist of HIV-1 proviral DNA[74]. Further, Kupffer cells harbor more HIV-1 strain than hepatocytes [75]. Therefore, the delivery of nanoparticles to macrophage with subsequent release into the hepatocytes containing T- lymphocytes is desirable for HIV treatment [76]. Each animal in group I was sacrificed after 24 h and fluorescent intensity in HIV infection associated organs were determined to quantify the uptake of DIR PLN (Figure 4.12). Accumulation of surrogate DIR PLN in different organs was observed in the order of spleen ≥ liver > lymph node > thymus > lungs >female reproductive tract (FRT)> heart > kidneys > brain after intravenous administration (Figure 4.11(c)). Availability of PLN to various tissue parenchyma credence upon modulation in nanoparticle size wherein; larger particles are phagocytosed by macrophagic cells including Kupffer cells (>200 nm) [77] and dendritic cells (>500 nm) in lymph nodes [78]. The average particle size of DIR PLN was 212.5±31.79 nm making particles <200 nm available to parenchymal cells of the liver, spleen, and lymph nodes. Higher biodistribution of DIR PLN in the spleen (15% T lymphocytes) and lymph nodes (75% T lymphocytes) amongst other organs harbouring latently infected T-lymphocyte was achieved. However, the fluorescent intensity was 4-fold higher in the spleen (HIV reservoir site) compared to the lymph node and thymus.

Route of administration reverberate LA potential of administered nanoformulation due to primary (injection site) and secondary (infiltered immune cells) depot genesis [9]. To this end, biodistribution studies of DIR PLN was assessed by subcutaneous (SC) administration. Only, 13.3±0.76% of the injected dose was biodistributed in RES and non-RES organs after 5 days as against 88.7±19.34% injected dose biodistributed to the whole body within 24h when administered intravenously. Furthermore, the primary depot was evident even at day 5 upon SC administration (Figure 4.11(b)) limning LA potential of developed PLN. Slow effective release of DIR PLN was confirmed by uniform biodistribution at day 3 post-administration. The

images of organs obtained after sacrificing animals of groups II, III, and IV at 1, 3, and 5-day post subcutaneous administration are represented in Figure 4.12.

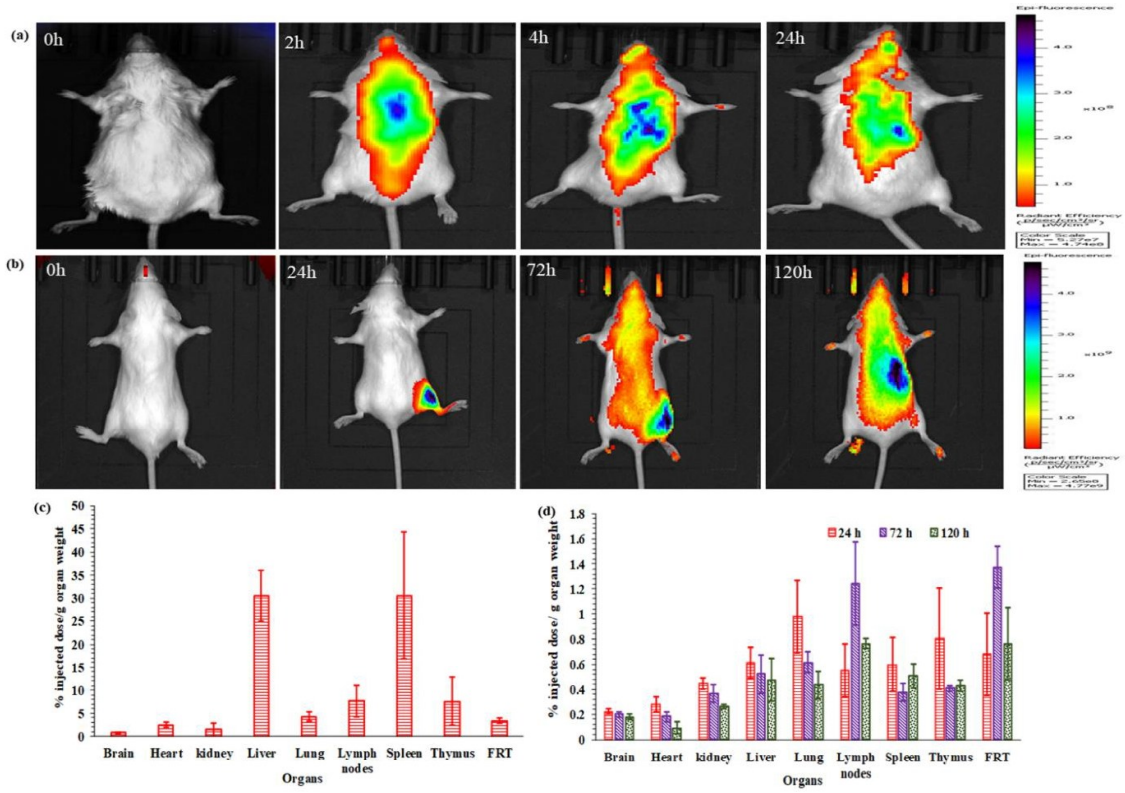

Figure 4.11 *In-vivo* biodistribution studies (a) Whole-body image after intravenous administration of DIR PLN at 0, 2, 4, and 24 h. (b) Whole-body image after subcutaneous administration of DIR PLN at 0, 24, 72, and 120 h (c) Biodistribution of DIR PLN in different organs after intravenous administration in 24 h. (d) Biodistribution of DIR PLN in different organs after subcutaneous administration in 24,72 and 120 h (Data represented as mean±SD, n=3)

Higher administration of DIR PLN in lymph node (containing 75% T lymphocyte) was obtained compared to the spleen in contrast to intravenous administration at day 3 post-administration. Sequestration of DIR PLN in lymph node was the aftermath of lymphatic uptake post-SC administration wherefrom the PLN would slowly be transported to the thoracic

duct and loaded into the systemic circulation. Similar observations were previously reported for combination drug nanoparticles of lopinavir, ritonavir, and tenofovir producing 3 waves in

plasma corresponding to fast (<8 h), intermediate (8-24 h), and protracted release (>48h-2 weeks) drug release through lymphatic-circulatory conjoint [11]. It was observed that DIR PLN accumulated and retained in infection spread site (lymph nodes) and reservoir sites (liver and spleen) after subcutaneous administration with total % injected dose/g organ weight of 2.56%, 2.25% and 1.99% after 1,3, and 5-day, respectively (Figure 4.11(d)). Previously LA slow-release rilpivirine nanocrystals were also localized in the liver, spleen, popliteal, and axillary lymph node after subcutaneous administration [79]. The biodistribution of DIR PLN was also observed in difficult-to-access locations including the brain due to carriage by secondary depot cells wherein; the % injected dose of DIR PLN/g organ weight was found to be 0.22%, 0.19% and 0.18% at 1, 3 and 5-day respectively post SC dosing. The tissue concentration of DIR PLN in the brain depicted no significant change until 5 days emphasizing the role of secondary depot forming monocytes which are customary to traverse through a privileged organ-like brain [80,81]. Therefore, enhanced lymphatic and brain uptake of DIR PLN would lead to the possible elimination of HIV relapse.

The % injected dose/g organ weight at HIV infection site (FRT) was found to be 0.67%, 1.37%, and 0.76% at 1^{st},3^{rd} and 5^{th} day respectively post subcutaneous dosing, suggesting wider potential in pre-exposure prophylaxis with an increase in PLN uptake up to 3^{rd} days (1.3±0.16%) at HIV infection site. Similar observations were reported previously for long-acting slow-release nanoformulation loaded with Tenofovir Alfanamide and Elvitegravir with great potential as pre-exposure prophylaxis wherein, 1.65-fold higher concentration of drug-loaded nanoparticles in the female reproductive tract was obtained compared to free drug and sustained release up to 336 h [25]. No significant difference ($p>0.05$) was observed in the fluorescence intensity at day 1 (group II), day 3 (group III), and day 5 (group IV), in each organ including RES organs, kidneys, heart, FRT, and brain underpinning long-acting slow

drug delivery potential of PLN. Nevertheless, the quantification of drugs in every organ is required to confirm the minimum effective concentration of drugs has been achieved.

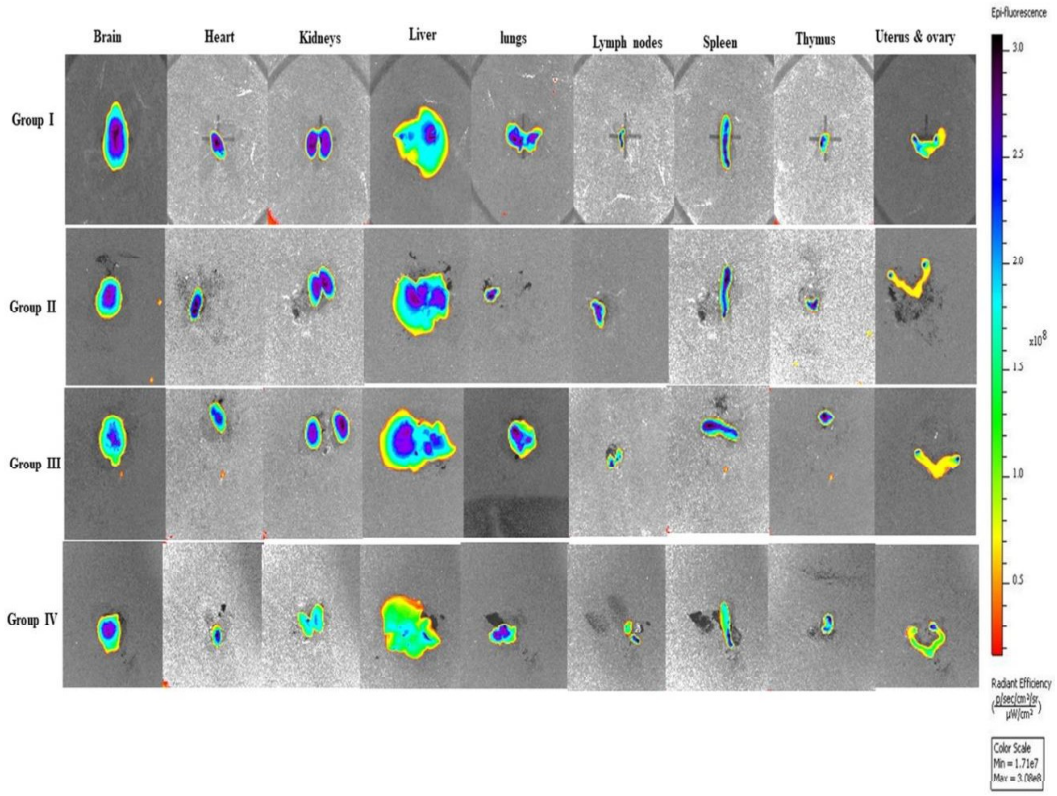

Figure 4.12. Images of the organs of the animals sacrificed at 24 h of group I, and 24 h, 72 h and 120 h of group II, III and IV respectively after DIR PLN administration via intravenous (group I) and subcutaneous route (group II, III and IV).

3.9 Prediction of dose and target site drug level by simulation of DIR PLN biodistribution profile

It is essential to attain the minimum effective drug concentration at the infection sites (e.g. spleen, lymph nodes, brain, and FRT) for complete eradication of the virus from the body. Infrared dye (e.g. DIR) loaded nanoparticles are most widely used as a surrogate to establish the biodistribution pattern of nanoparticles by bio-imaging of live animals. However, this sophisticated high-throughput technique does not provide actual available tissue level of the drugs which is necessary to define drug concentration at the injection site.

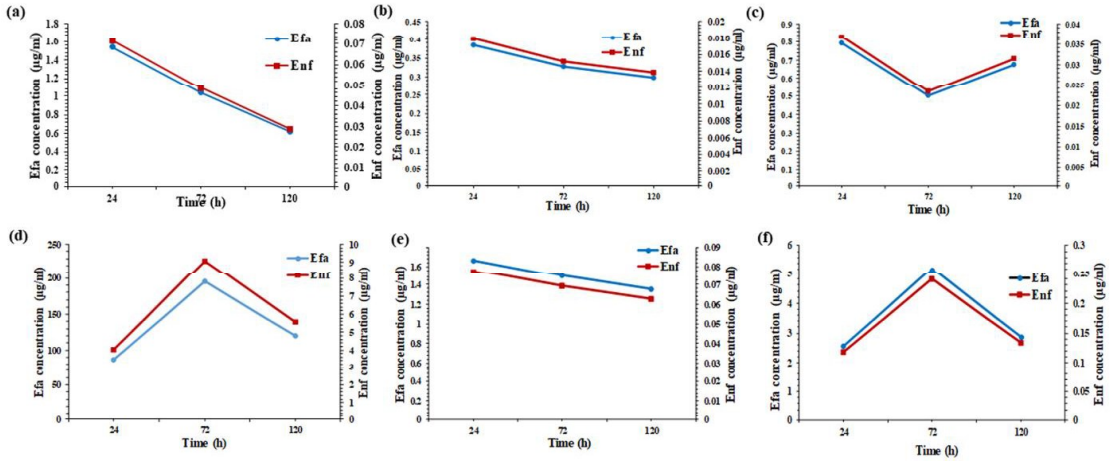

Figure 4.13. Simulated Efavirenz and Enfuvirtide concentration in different organs (a) draining organs (heart, lungs and kidneys) (b) liver (c) spleen (d) lymph node (e) brain (f) female reproductive tract

In the present study, we attempted to predict the available drug levels at target sites by simulation of the DIR PLN biodistribution profile. The model predicted a significantly higher concentration of both Efa and Enf in the lymph node upon SC administration. A higher amount of sequestered PLN in macrophages and T-lymphocytes of lymph node might have led to slow effective release into the lymphatic vesicles thereby draining into the thoracic duct and presentation into the systemic circulation. The secondary immune cell depot once into systemic circulation cause protracted drug release after differentiating into various tissues depending upon the differential blood flow volume to each organ [10,11]. Furthermore, the order of predicted available tissue concentration female reproductive tract>brain>draining organ>spleen>liver. Predicted higher amounts of available Efa and Enf in the female reproductive tract (major infection site) and brain (most inaccessible organ) could be attributed to higher blood volume containing secondary depot to these organs. Furthermore, the predicted available tissue concentration of Efa (EC_{50}- 2 nM) and Enf (EC_{50}- 6-91 nM) were found to be higher than the effective concentration in all the organs (Figure 4.13) until day 5 for an administered dose of PLN equivalent to 1250 µg and 58.17 µg of Efa and Enf respectively.

Nevertheless, preclinical studies have yet to be performed to establish accurate tissue concentration and efficacy of the formulation.

4. Conclusion

The current study is the first proof of concept of long-acting potential for novel cARV namely; Efa and Enf when loaded into PLN. Furthermore, Efa-Enf PLN depicted enhanced intracellular delivery to established secondary depot and hub for transcriptionally dormant form of HIV-1 which include macrophage and T-cells. Additionally, it highlights the implication of subcutaneous administration for week long protracted drug release through secondary depot in systemic circulation preceded via lymphatic route which could be well corroborated with *in-vitro* drug release of Efa and Enf from PLN. The distinctive long-acting contrivance of surrogate PLN caused sustained delivery to major infection, spread, and reservoir sites. Furthermore, blood flow to specific organs inflect the biodistribution of PLN available in secondary depot. To this end, correlation studies have been performed as the first illustration to estimate the dose of Efa-Enf PLN desirable for establishing the required tissue concentration of Efa and Enf in each organ which would be lucrative in preserving time and cost during preclinical studies.

References

[1] M. Smit, C. Smit, S. Geerlings, L. Gras, K. Brinkman, T.B. Hallett, F. De Wolf, A. Observational, Changes in First-Line cART Regimens and Short-Term Clinical Outcome between 1996 and 2010 in The Netherlands, PLoS One. 8 (2013) 1–10. doi:10.1371/journal.pone.0076071.

[2] M. Delaney, History of HAART – the true story of how effective multi-drug therapy

was developed for treatment of HIV disease, Retrovirology. 3 (2006) S6. doi:10.1186/1742-4690-3-S1-S6.

[3] A. Sosnik, R. Augustine, Challenges in oral drug delivery of antiretrovirals and the innovative strategies to overcome them ☆, Adv. Drug Deliv. Rev. 103 (2016) 105–120. doi:10.1016/j.addr.2015.12.022.

[4] J.B. Nachega, V.C. Marconi, G.U. Van Zyl, E.M. Gardner, W. Preiser, S.Y. Hong, E.J. Mills, R. Gross, C. Town, S. Africa, HIV Treatment Adherence, Drug Resistance, Virologic Failure: Evolving Concepts, Infect Disord Drug Targets. 11 (2011) 167–174.

[5] M. Roser, R. Hannah, HIV / AIDS, (2019). https://ourworldindata.org/hiv-aids (accessed April 17, 2020).

[6] B.J. Aungst, P-glycoprotein, secretory transport, and other barriers to the oral delivery of anti-HIV drugs, Adv. Drug Deliv. Rev. 39 (1999) 105–116.

[7] and H.E.G. Benson J Edagwa, Tian Zhou, JoEllyn M McMillan, Xin-Ming Liu, Development of HIV Reservoir Targeted Long Acting Nanoformulated Antiretroviral Therapies, Curr Med Chem. 21 (2014) 4186–4198.

[8] A. Owen, S. Rannard, Strengths, weaknesses, opportunities and challenges for long acting injectable therapies: Insights for applications in HIV therapy, Adv. Drug Deliv. Rev. 103 (2016) 144–156. doi:10.1016/j.addr.2016.02.003.

[9] D.H. Surve, A.B. Jindal, Recent advances in long-acting nanoformulations for delivery of antiretroviral drugs, J. Control. Release. 324 (2020) 379–404. doi:10.1016/j.jconrel.2020.05.022.

[10] T. Zhou, H. Su, P. Dash, Z. Lin, B. Laxmi, D. Shetty, T. Kocher, A. Szlachetka, B.

Lamberty, H.S. Fox, L. Poluektova, S. Gorantla, J. Mcmillan, N. Gautam, R.L. Mosley, Y. Alnouti, B. Edagwa, H.E. Gendelman, Creation of a nanoformulated cabotegravir prodrug with improved antiretroviral profiles, Biomaterials. 151 (2018) 53–65. doi:10.1016/j.biomaterials.2017.10.023.

[11] J. Kraft, L. McConnachie, J. Koehn, L. Kinman, J. Sun, A. Collier, C. Collins, D. Shen, R. Ho, Mechanism-based pharmacokinetic (MBPK) models describe the complex plasma kinetics of three antiretrovirals delivered by a long-acting anti-HIV drug combination nanoparticle formulation, J. Control. Release. 275 (2018) 229–241. doi:10.1016/j.jconrel.2018.02.003.

[12] Janssen Announces Health Canada Approval of CABENUVA™, the First Long-Acting Regimen for the Treatment of HIV, (2020). https://www.jnj.com/janssen-announces-health-canada-approval-of-cabenuva-the-first-long-acting-regimen-for-the-treatment-of-hiv (accessed May 11, 2020).

[13] D.A. Margolis, J. Gonzalez-garcia, H. Stellbrink, J.J. Eron, Y. Yazdanpanah, D. Podzamczer, T. Lutz, J.B. Angel, G.J. Richmond, B. Clotet, F. Gutierrez, L. Sloan, M.S. Clair, M. Murray, S.L. Ford, J. Mrus, P. Patel, H. Crauwels, S.K. Griffith, K.C. Sutton, D. Dorey, K.Y. Smith, P.E. Williams, W.R. Spreen, Long-acting intramuscular cabotegravir and rilpivirine in adults with HIV-1 infection (LATTE-2): 96-week results of a randomised , open-label , phase 2b , non-inferiority trial, Lancet. 6736 (2017) 1–12. doi:10.1016/S0140-6736(17)31917-7.

[14] S. Mandal, P.K. Prathipati, G. Kang, Y. Zhao, Z. Yuan, W. Fan, Q. Li, C. Destache, Tenofovir alafenamide and elvitegravir loaded nanoparticles for long-acting prevention of HIV-1 vaginal transmission, AIDS. 31 (2018) 469–476. doi:10.1097/QAD.0000000000001349.Tenofovir.

[15] S. Mandal, G. Kang, P. Kumar, Y. Zhou, W. Fan, Q. Li, C.J. Destache, Nanoencapsulation introduces long-acting phenomenon to tenofovir alafenamide and emtricitabine drug combination: A comparative pre-exposure prophylaxis efficacy study against HIV-1 vaginal transmission, J. Control. Release. 294 (2019) 216–225. doi:10.1016/j.jconrel.2018.12.027.

[16] S. Mandal, M. Belshan, A. Holec, Y. Zhou, C. Destache, An Enhanced Emtricitabine-Loaded Long-Acting Nanoformulation for Prevention or Treatment of HIV Infection, Antimicrob. Agents Chemother. 61 (2017) 1–11.

[17] J. Freeling, J. Koehn, C. Shu, J. Sun, R. Ho, Anti-HIV Drug-Combination Nanoparticles Enhance as Well as Triple-Drug Combination Levels in Cells Within Lymph Nodes and Blood in Primates, AIDS Res. Hum. Retrviruses. 31 (2015) 107–114. doi:10.1089/aid.2014.0210.

[18] J. Duan, J.P. Freeling, J. Koehn, C. Shu, R.J.Y. Ho, Evaluation of Atazanavir and Darunavir Interactions with Lipids for Developing pH-responsive Anti-HIV Drug Combination Nanoparticles, J Pharm Sci. 103 (2014) 2520–2529. doi:10.1002/jps.24046.Evaluation.

[19] J. Freeling, J. Koehn, C. Shu, J. Sun, R. Ho, Long-acting three-drug combination anti-HIV nanoparticles enhance drug exposure in primate plasma and cells within lymph nodes and blood, AIDS. 28 (2014) 2625–2631.

[20] J.R. Hilaire, A.N. Bade, B. Sillman, N. Gautam, J. Herskovitz, B. Laxmi, D. Shetty, M.S. Wojtkiewicz, A. Szlachetka, B.G. Lamberty, S. Sravanam, H.S. Fox, Y. Alnouti, P.K. Dash, J.M. Mcmillan, B.J. Edagwa, H.E. Gendelman, Creation of a long-acting rilpivirine prodrug nanoformulation, J. Control. Release. 311–312 (2019) 201–211.

doi:10.1016/j.jconrel.2019.09.001.

[21] Z. Lin, N. Gautam, Y. Alnouti, J. Mcmillan, A.N. Bade, H.E. Gendelman, B. Edagwa, ProTide generated long-acting abacavir nanoformulations, Chem. Commun. 54 (2018) 8371–8374. doi:10.1039/c8cc04708a.

[22] D. Guo, T. Zhou, M. Araínga, D. Palandri, N. Gautam, T. Bronich, Y. Alnouti, J. Mcmillan, B. Edagwa, H.E. Gendelman, Creation of a Long-Acting Nanoformulated 2',3'-Dideoxy-3'-Thiacytidine, J Acquir Immune Defic Syndr. 74 (2017) 75–83.

[23] P. Puligujja, S.S. Balkundi, L.M. Kendrick, H.M. Baldridge, J.R. Hilaire, A.N. Bade, P.K. Dash, G. Zhang, L.Y. Poluektova, S. Gorantla, X. Liu, T. Ying, Y. Feng, Y. Wang, D.S. Dimitrov, J.M. Mcmillan, H.E. Gendelman, Pharmacodynamics of long-acting folic acid-receptor targeted ritonavir-boosted atazanavir nanoformulations, Biomaterials. 41 (2015) 141–150. doi:10.1016/j.biomaterials.2014.11.012.

[24] S. Perazzolo, L.M. Shireman, L.A. Mcconnachie, J.C. Kraft, D.D. Shen, R.J.Y. Ho, Three HIV Drugs , Atazanavir , Ritonavir , and Tenofovir , Coformulated in Drug-Combination Nanoparticles Exhibit Long-Acting and Lymphocyte-Targeting Properties in Nonhuman Primates, J. Pharmceutical Sci. 101 (2018) 1–10. doi:10.1016/j.xphs.2018.07.032.

[25] P.K. Prathipati, S. Mandal, G. Pon, R. Vivekanandan, C.J. Destache, Pharmacokinetic and Tissue Distribution Profile of Long Acting Tenofovir Alafenamide and Elvitegravir Loaded Nanoparticles in Humanized Mice Model, Pharm Res. 34 (2017) 2749–2755. doi:10.1007/s11095-017-2255-7.

[26] S. Mandal, G. Kang, P. Kumar, Y. Zhou, W. Fan, Q. Li, C.J. Destache, Nanoencapsulation introduces long-acting phenomenon to tenofovir alafenamide and

emtricitabine drug combination : A comparative pre- exposure prophylaxis e ffi cacy study against HIV-1 vaginal transmission, J. Control. Release. 294 (2019) 216–225. doi:10.1016/j.jconrel.2018.12.027.

[27] S. Mandal, G. Kang, P. Kumar, W. Fan, Q. Li, C.J. Destache, Long-acting parenteral combination antiretroviral loaded nano-drug delivery system to treat chronic HIV-1 infection : A humanized mouse model study, Antiviral Res. 156 (2018) 85–91. doi:10.1016/j.antiviral.2018.06.005.

[28] B.M. Best, M. Goicoechea, Efavirenz-Still first line king?, Expert Opin Drug Metab Toxicol. 4 (2008) 965–972. doi:10.1517/17425255.4.7.965.Efavirenz.

[29] H. Raina, S. Kaur, A.B. Jindal, Development of efavirenz loaded solid lipid nanoparticles: Risk assessment, quality-by-design (QbD) based optimisation and physicochemical characterisation, J. Drug Deliv. Sci. Technol. 39 (2017) 180–191. doi:10.1016/j.jddst.2017.02.013.

[30] V. Makwana, R. Jain, K. Patel, M. Nivsarkar, A. Joshi, Solid lipid nanoparticles (SLN) of Efavirenz as lymph targeting drug delivery system: Elucidation of mechanism of uptake using chylomicron flow blocking approach, Int. J. Pharm. 495 (2015) 439–446. doi:10.1016/j.ijpharm.2015.09.014.

[31] J. Labonte, J. Lebbos, P. Kirkpatrick, Enfuvirtide, Nat. Rev. Drug Discov. 2 (2003) 345–346. doi:10.1038/nrd1091.

[32] P.L. Vernazza, P. Schmid, Antiviral drugs, Elsevier B.V., 2005. doi:10.1016/S0378-6080(05)80451-9.

[33] H. Hardy, P. Skolnik, Enfuvirtide , a New Fusion Inhibitor for Therapy of Human Immunodeficiency Virus Infection, Pharmacotherapy. 24 (2004) 198–211.

[34] I.H. Patel, X. Zhang, K. Nieforth, M. Salgo, N. Buss, Pharmacokinetics, pharmacodynamics and drug interaction potential of enfuvirtide, Clin. Pharmacokinet. 44 (2005) 175–186. doi:10.2165/00003088-200544020-00003.

[35] Fuzeon (enfuvirtide) for Injection, (2003). https://www.accessdata.fda.gov/drugsatfda_docs/label/2018/021481s032lbl.pdf (accessed April 29, 2020).

[36] Enfuvirtide, (n.d.). https://pubchem.ncbi.nlm.nih.gov/compound/Enfuvirtide (accessed June 17, 2018).

[37] Enfuvirtide, (n.d.). https://www.drugbank.ca/drugs/DB00109 (accessed July 30, 2017).

[38] J. Wen, Li Fei, Yu Qian, Wang Qianqian, Qi Shan, Su Lan, Xie Le, Le Shibo, Co-delivery of HIV-1 entry inhibitor and NNRTI shuttled by nanoparticles: cocktail therapeutics strategy for antiviral therapy, AIDS. (2015). doi:10.1097/QAD.0000000000000971.

[39] A. Mukherjee, K. Waters, P. Kalyan, A.S. Achrol, Lipid-polymer hybrid nanoparticles as a next- generation drug delivery platform: state of the art, emerging technologies, and perspectives, Int. J. Nanomedicine. 14 (2019) 1937–1952.

[40] T. Nayab, M. Muhammad Tahir, Haseeb Asadullah, P. Farzana, K. Muhammad Muzamil, K. Safiullah, J. Nasrullah, K. Arshad, Lipid Polymer Hybrid Nanoparticles: A Novel Approach for Drug Delivery, in: Role Nov. Drug Deliv. Veh. Nanobiomedicine, 2019.

[41] M. Gallarate, M. Trotta, L. Battaglia, D. Chirio, Preparation of solid lipid nanoparticles from W/O/W emulsions: Preliminary studies on insulin encapsulation, J. Microencapsul. 26 (2009) 394–402. doi:10.1080/02652040802390156.

[42] D.H. Surve, A.B. Jindal, Development and validation of reverse-phase high-performance liquid chromatographic (RP-HPLC) method for quantification of Efavirenz in Efavirenz-Enfuvirtide co-loaded polymer-lipid hybrid nanoparticles, J. Pharm. Biomed. Anal. 175 (2019) 112765. doi:10.1016/j.jpba.2019.07.013.

[43] K.S. Joshy, S. Snigdha, N. Kalarikkal, L.A. Pothen, S. Thomas, Gelatin modified lipid nanoparticles for anti retroviral drug delivery, Elsevier Ireland Ltd, 2017. doi:10.1016/j.chemphyslip.2017.07.002.

[44] G. Chen, J. Wen, Poly(lactic-co-glycolic acid) based double emulsion nanoparticle as a carrier system to deliver glutathione sublingually, J. Biomed. 3 (2018) 50–59. doi:10.7150/jbm.27148.

[45] E.C. Gryparis, G. Mattheolabakis, D. Bikiaris, K. Avgoustakis, Effect of conditions of preparation on the size and encapsulation properties of PLGA-mPEG nanoparticles of cisplatin, Drug Deliv. 14 (2007) 371–380. doi:10.1080/10717540701202937.

[46] D.L. Cooper, S. Harirforoosh, Effect of formulation variables on preparation of celecoxib loaded polylactide-co-glycolide nanoparticles, PLoS One. 9 (2014) 1–22. doi:10.1371/journal.pone.0113558.

[47] J. Hao, X. Fang, Y. Zhou, J. Wang, F. Guo, F. Li, X. Peng, Development and optimization of solid lipid nanoparticle formulation for ophthalmic delivery of chloramphenicol using a Box-Behnken design., Int. J. Nanomedicine. 6 (2011) 683–692. doi:10.2147/IJN.S17386.

[48] S. Pradhan, J. Hedberg, E. Blomberg, S. Wold, I. Odnevall Wallinder, Effect of sonication on particle dispersion, administered dose and metal release of non-functionalized, non-inert metal nanoparticles, J. Nanoparticle Res. 18 (2016) 1–14.

doi:10.1007/s11051-016-3597-5.

[49] D. Cun, D.K. Jensen, M.J. Maltesen, M. Bunker, P. Whiteside, D. Scurr, C. Foged, H.M. Nielsen, High loading efficiency and sustained release of siRNA encapsulated in PLGA nanoparticles: Quality by design optimization and characterization, Eur. J. Pharm. Biopharm. 77 (2011) 26–35. doi:10.1016/j.ejpb.2010.11.008.

[50] F.W.H. Kruger, W.J. McGill, A DSC Study of Curative Interactions., J. Appl. Polym. Sci. 42 (1991) 2643–2649.

[51] N. Passerini, D.Q.M. Craig, An investigation into the effects of residual water on the glass transition temperature of polylactide microspheres using modulated temperature DSC, 73 (2001) 111–115.

[52] L. Liu, K. Mao, W. Wang, H. Pan, F. Wang, M. Yang, H. Liu, Kolliphor ® HS 15 Micelles for the Delivery of Coenzyme Q10 : Preparation , Characterization , and Stability, AAPS PharmSciTech. 17 (2016). doi:10.1208/s12249-015-0399-5.

[53] N. Verhoeven, T. Loon, T. Furuta, C. Yamamoto, T. Ohashi, H. Yoshii, Characteristics of dehydration kinetics of dihydrate trehalose to its anhydrous form in ethanol by DSC, Food Chem. 132 (2012) 1638–1643. doi:10.1016/j.foodchem.2011.06.010.

[54] Y. Ding, K.A. Nielsen, B.P. Nielsen, N.W. Bøje, R.H. Müller, S. Min, Lipid-drug-conjugate (LDC) solid lipid nanoparticles (SLN) for the delivery of nicotine to the oral cavity – Optimization of nicotine loading e ffi ciency, Eur. J. Pharm. Biopharm. 128 (2018) 10–17. doi:10.1016/j.ejpb.2018.03.004.

[55] M.J. Ansari, K. Anwer, S. Jamil, R. Al-shdefat, B.E. Ali, M.M. Ahmad, M.N. Ansari, Enhanced oral bioavailability of insulin-loaded solid lipid nanoparticles : pharmacokinetic bioavailability of insulin-loaded solid lipid nanoparticles in diabetic

rats, Drug Deliv. 00 (2015) 1–8. doi:10.3109/10717544.2015.1039666.

[56] D. Romani, S. Beatriz, S.A. Branda, Structural and vibrational characterization of anhydrous and dihydrated species of trehalose based on the FTIR and FTRaman spectra and DFT calculations, (2018) 229–249. doi:10.1016/j.jksus.2017.01.009.

[57] A. Azizi, B. Ranjbar, Plasmonic Circular Dichroism Study of DNA – Gold Nanoparticles Bioconjugates, Plasmonics. (2014) 273–281. doi:10.1007/s11468-013-9620-0.

[58] T. Jerez, M.-L. Tan, T. Ichiye, Solvation of Glucose, Trehalose and Sucrose by the Soft Sticky Dipole-Quadrupole-Octupole Water model, Chem Phys Lett. 491 (2010) 218–223. doi:10.1016/j.cplett.2010.04.020.Solvation.

[59] M. Brzezi, M. Socka, B. Kost, Microfluidics for producing polylactide nanoparticles and microparticles and their, Polym. Int. 68 (2019) 997–1014. doi:10.1002/pi.5753.

[60] G. Lindsay, S. Crowe, J. McCarthy, K. Mills, J. Mouton, R. Norrby, D. Paterson, M. Pfaller, The Use of Antibiotics, 2012.

[61] S. Huang, S. Lin, S. Chang, Y. Lin, C. Chiang, Prediction of plasma efavirenz concentrations among HIV- positive patients taking efavirenz- containing combination antiretroviral therapy, Sci. Rep. (2017) 1–9. doi:10.1038/s41598-017-16483-2.

[62] S. Cheng, Y. Wang, Z. Zhang, X. Lv, G.F. Gao, Y. Shao, L. Ma, X. Li, Enfuvirtideĝ'PEG conjugate: A potent HIV fusion inhibitor with improved pharmacokinetic properties, Eur. J. Med. Chem. 121 (2016) 232–237. doi:10.1016/j.ejmech.2016.05.027.

[63] W. Lee, K.M. Frey, R. Gallardo-macias, K.A. Spasov, M. Bollini, K.S. Anderson, W.L. Jorgensen, Picomolar Inhibitors of HIV-1 Reverse Transcriptase: Design and

Crystallography of Naphthyl Phenyl Ethers, (2014). doi:10.1021/ml5003713.

[64] S.W. Morton, M.J. Lee, Z.J. Deng, E.C. Dreaden, E. Siouve, K.E. Shopsowitz, N.J. Shah, M.B. Yaffe, P.T. Hammond, A Nanoparticle-Based Combination Chemotherapy Delivery System for Enhanced Tumor Killing by Dynamic Rewiring of Signaling Pathways, Sci Signal. 7 (2014). doi:10.1126/scisignal.2005261.A.

[65] V. Burlui, M. Popa, A.N. Cadinoiu, C. Stadoleanu, V. Zamaru, L. Dârţu, E. Folescu, D.M. Raţă, Physico-chemical characterization and in vitro haemolysis evaluation of titanium dioxide nanoparticles, 5 (2015).

[66] A.R. Kallianpur, Q. Wang, P. Jia, T. Hulgan, Z. Zhao, S.L. Letendre, R.J. Ellis, R.K. Heaton, D.R. Franklin, J. Barnholtz-sloan, A.C. Collier, C.M. Marra, D.B. Clifford, B.B. Gelman, J.C. Mcarthur, S. Morgello, Anemia and Red Blood Cell Indices Predict HIV-Associated Neurocognitive Impairment in the Highly Active Antiretroviral Therapy Era, J. Infect. Dis. 213 (2016) 1065–1073. doi:10.1093/infdis/jiv754.

[67] K.H.K. Wong, R.D. Sandlin, T.R. Carey, K.L. Miller, A.T. Shank, R. Oklu, S. Maheswaran, D.A. Haber, D. Irimia, S.L. Stott, M. Toner, The Role of Physical Stabilization in Whole Blood Preservation, Sci. Rep. 6 (2016) 1–9. doi:10.1038/srep21023.

[68] E. Zvetkova, D. Fuchs, Medical significance of simultaneous application of red blood cell distribution width (RDW) and neopterin as diagnostic/prognostic biomarkers in clinical practice, Pteridines. 28 (2017) 133–140.

[69] C. Gavegnano, R. Schinazi, Antiretroviral therapy in macrophages: implication for HIV eradication, Antivir Chem Chemother. 20 (2010) 63–78. doi:10.3851/IMP1374.Antiretroviral.

[70] Z. Kruize, N.A. Kootstra, The Role of Macrophages in HIV-1 Persistence and Pathogenesis, Front. Microbiol. 10 (2019) 1–17. doi:10.3389/fmicb.2019.02828.

[71] D. Surve, P. Dandekar, P. Devarajan, A. Jindal, Intracellular Delivery: An Overview, in: Target. Intracell. Drug Deliv. by Recept. Mediat. Endocytosis, 2019: pp. 3–44.

[72] E. Majorovits, M. Nejmeddine, Y. Tanaka, G.P. Taylor, S.D. Fuller, C.R.M. Bangham, Human T-Lymphotropic Virus-1 Visualized at the Virological Synapse by Electron Tomography, PLoS One. 3 (2008) 1–10. doi:10.1371/journal.pone.0002251.

[73] M. V Beccari, B.T. Mogle, E.F. SIdman, K.A. Mastro, E.A. Reddy, W.D. Kufel, Ibalizumab , a Novel Monoclonal Antibody for the Management of Multidrug-Resistant HIV-1 Infection, Antimicrob. Agents Chemother. 63 (2019) 1–12.

[74] F. Hufert, J. Schmitz, M. Schreiber, H. Schmitz, P. Racz, D. Laer, Human Kupffer cells infected with HIV-1, J. Acquir. Immune Defic. Syndr. (1993) 772–777.

[75] C. Housset, P.M. Girard, J. Leibowitch, A.G. Saimot, C. Brichot, C. Bernard, lmmunohistochemical Evidence for Human lmmunodeficiency Virus-l Infection of Liver Kupffer Cells, Hum. Pathol. 21 (1990) 404–408.

[76] L. Jiang, T. Wang, Y. Wang, Z. Wang, Y. Bai, Co-disposition of chitosan nanoparticles by multi types of hepatic cells and their subsequent biological elimination : the mechanism and kinetic studies at the cellular and animal levels, Int. J. Nanomedicine. 14 (2019) 6035–6060.

[77] D. Chow, J. Hwang, Targeting Small Unilamellar Cells by Dose Effect1 Liposomes to Hepatic Parenchymal, J. Pharmcology Exp. Ther. 248 (1989) 506–513.

[78] T.Z. Chang, S.S. Stadmiller, E. Staskevicius, J.A. Champion, Effects of Ovalbumin Protein Nanoparticle Vaccine Size and Coating on Dendritic Cell Processing, Niomater

Sci. 5 (2017) 223–233. doi:10.1039/c6bm00500d.Effects.

[79] B.M. Ottemann, A.J. Helmink, W. Zhang, I. Mukadam, C. Woldstad, J.R. Hilaire, Y. Liu, J.M. Mcmillan, B.J. Edagwa, R.L. Mosley, J.C. Garrison, B.D. Kevadiya, H.E. Gendelman, Bioimaging predictors of rilpivirine biodistribution and antiretroviral activities, Biomaterials. 185 (2018) 174–193. doi:10.1016/j.biomaterials.2018.09.018.

[80] N.L. Klyachko, R. Polak, M.J. Haney, Y. Zhao, J.G. Neto, M.C. Hill, A. V Kabanov, R.E. Cohen, F. Rubner, E. V Batrakova, C. Hill, M.V.L.M. State, Macrophages with cellular backpacks for targeted drug delivery to the brain, Biomaterials. 140 (2017) 79–87. doi:10.1016/j.biomaterials.2017.06.017.Macrophages.

[81] W. He, N. Kapate, C.W.S. Iv, Drug delivery to macrophages : A review of targeting drugs and drug carriers to macrophages for inflammatory diseases, Adv. Drug Deliv. Rev. (2019). doi:10.1016/j.addr.2019.12.001.